EXPERIMENTAL AND MODELING APPROACHES TO UNDERSTAND EFFECTS OF COMBINED LOADING IN RELATION TO PRESSURE ULCER FORMATION

By

Abinand Manorama

A DISSERTATION

Submitted to
Michigan State University
in partial fulfillment of the requirements
for the degree of

Mechanical Engineering – Doctor of Philosophy

2013

ABSTRACT

EXPERIMENTAL AND MODELING APPROACHES TO UNDERSTAND EFFECTS OF COMBINED LOADING IN RELATION TO PRESSURE ULCER FORMATION

By

Abinand Manorama

Forces applied to the skin cause a decrease in regional blood flow which can result in tissue necrosis and lead to the formation of deep, penetrating wounds called pressure ulcers. Although surface pressure is known to be a primary risk factor for developing a pressure ulcer, a seated individual rarely experiences pressure alone but rather combined loading which includes pressure as well as shear force on the skin. However, little research has been conducted to quantify the effects of shear forces on blood flow.

Also, deformation of cells in its own right can cause individual cell death leading to tissue necrosis and the formation of a pressure ulcer. It is unclear if ulcers start at the skin level and proceed inwards toward the muscle, or if they start at the muscular level and propagate to the dermal and epidermal regions. Thus, there is a need to study deformation at the deep as well as superficial level to better understand the mode and direction of pressure ulcer propagation.

The goals of this research were to: i) determine the effects of normal and combined loads on arterial and venous blood flow in the forearm; ii) understand the possible mode and direction of tissue necrosis; iii) develop an approach to model arterial to venous blood flow in order to better understand the effects of forces on blood flow; iv) determine the relation of soft tissue thickness and local skin temperature with blood flow at varied load conditions.

To address the first goal, human participants were tested in a MRI scanner under no load, normal load, and a combination of normal and shear loads. Arterial and venous blood flow changes in the forearm were measured using phase-contrast imaging. Results showed that blood flow decreased due to normal loads, and decreased further with combined loads.

To address the second goal, a subject-specific 3D model of the forearm section was developed from MR images, and the effects of normal and shear forces were evaluated through FE analysis. Results showed that combined forces caused increased stresses and strains in skin and muscle when compared to normal forces alone.

The third goal was addressed by creating three models based on deformation geometry and simulating arterial to venous blood flow by assuming muscle tissue to be permeable to blood flow. Results showed that muscle permeability decreased with the application of normal loads, and decreased further with the addition of shear loads.

Finally, the relation between soft tissue thickness and blood flow under varied loads as well as the relation between local skin temperature and skin perfusion under varied loads were explored. Results showed that a smaller magnitude of soft tissue thickness was related to reduced blood flow under combined loading. Increased skin temperatures were also more detrimental to blood flow under combined loading. Thus, shear force is an important factor to consider in relation to tissue necrosis and hence to pressure ulcer formation, and future prevention approaches should address shear loads.

To my Twin Flame

ACKNOWLEDGEMENTS

I have had the pleasure of associating with many wonderful people over the last few years, and each of these people has played a significant role in shaping my career.

First of all, I would like to express my gratitude to my research advisor, Dr. Tamara Reid Bush, who got me off on the right foot at the start of my graduate studies and continued to guide and support me in my academic endeavor till date. I am very thankful to my PhD committee members, Dr. Seungik Baek, Dr. Neil Wright, and Dr. Ron Meyer for lending their support, and providing crucial feedback on my research. My colleagues at the Biomechanical Design Research Laboratory, Sam Leitkam, Brad Rutledge, Josh Drost, Jessica Buschman, Mike Aurino, and the rest of the group deserve special thanks for providing a stimulating intellectual work environment, and for their help and assistance through the years.

Special thanks go out to Kimberly Whinna Cottrell, Brian Pene, and Arthur Harsuvanakit at Autodesk, who made my stay in San Francisco a very memorable one. I would also like to acknowledge the rest of team at Autodesk, with a special mention to Chris Hall, Rita Schnipke, James Neville, and James Herzing for their expert support in my modeling work.

I would like to acknowledge my friends, Avinash Jammalamadaka and Venkat Ramakrishnan for the multiple brainstorming sessions we have had, and also for the many good times we have shared. A very special acknowledgment goes to Anchita Monga, Raghav Prashant Sundar, Ezhiylmurugan Rangasamy, and Uthaya Natarajan for being my support system and sticking with me through thick and thin until this day. Several other friends also deserve special mention, including Divya Gunaseelan, Nikita Sharma, Amrita Oak, Sudhanwa Dewasthale, Anju

Kurian, Satish Nallapaneni, Kishore Janardhanan, Mohit Patil, Madhumitha Sivaraman, Rengarajan Shanmugam , and Amal Ibourk.

Last but not the least, I would like to express my gratitude to my parents, Mr. Anbazhagan, and Mrs. Manorama, and my brother Aravind for their endless love, and for supporting and encouraging me in all my endeavors.

TABLE OF CONTENTS

LIST OF TABLES

LIST OF FIGURES

1. INTRODUCTION

Pressure ulcers are regions of tissue breakdown in the skin and underlying muscles. Many individuals develop pressure ulcers, including the elderly, those with a spinal cord injury, and the bedridden. Although many factors are believed to play a role in the development of these wounds, the most widely studied is the normal force, or the pressure that results from the normal force. Other important factors include shear force, temperature, and soft tissue thicknesses (i.e. skin, fat, muscle). Although, the effects of normal forces have been well studied in literature, research on other factors and their combined effects is sparse.

There are two schools of thought about the mechanism of pressure ulcer initiation and propagation. One school of thought states that forces of the body against an external support surface such as a wheelchair or a bed cause a decrease in blood flow to the skin and underlying tissues, which leads to tissue necrosis, thus causing a pressure ulcer. The other theory states that the external forces cause higher internal stresses and would lead to tissue necrosis and hence to pressure ulcers due to deformation of the cells, independent of blood flow. Additionally, it is not clear in which direction a pressure ulcer propagates. The commonly agreed theory is that a pressure ulcer starts at the skin level, and proceeds deeper through the muscle, to the bone. The other theory is that the ulcer starts inside, at the bone-muscle interface, and proceeds towards the surface of the skin. Additional research is necessary to determine where tissue damage is most likely to originate and thus which direction of propagation is more likely. Alternatively, if conditions for tissue damage are located both at superficial and deep regions, then both theories have equal probability.

The overall goal of this research was to better understand how blood perfusion, deeper vessel blood flow rates, and internal stresses and strains changed between conditions with no load, normal load, and combined loads of normal and shear. This knowledge will help in understanding the effect that shear forces have in pressure ulcer formation, in addition to understanding the mode and direction of pressure ulcer initiation and propagation. Also, the relations of soft tissue thickness and local skin temperature with blood flow at various loads were explored.

The following chapters narrate the specific goals, methods, and findings of this research. The chapters are prepared in the form of journal publications and therefore, each chapter contains an introduction, methods, results and discussion section.

Chapter 2 discusses research that was conducted to determine the effects of externally applied forces on the arterial and venous blood flow in the forearm. Human participants were tested in a Magnetic Resonance Imaging (MRI) scanner, and their blood flow monitored using Phase Contrast Magnetic Resonance Imaging (PC-MRI). Normal and shear forces were applied and the corresponding changes in blood flow were analyzed. This study has been published in *Clinical Biomechanics*, a science-indexed journal.

Chapter 3 describes research that was conducted to better understand the likely mode of tissue necrosis (i.e. location of the initiation of tissue damage) due to internal stresses and deformation. For this work a subject-specific 3D finite element (FE) model of a forearm section was developed from MR images, and a deformation analysis was performed on the model. The model was comprised of skin, muscle, and bones. The effects of experimentally applied normal and shear forces on internal stresses and deformation were evaluated through FE analysis. The total deformation values from simulation results were compared with those in the MRI slices.

Chapter 4 introduces the development and demonstration of an approach inspired by mathematical methods associated with groundwater flow. This approach was used to model the arterial to venous blood flow in the forearm. For this analysis, the muscle was assumed to be permeable to blood flow, and a muscle permeability value was calculated for three loading conditions.

Chapter 5 describes research conducted to determine the relation of soft tissue thickness and skin temperature with blood flow changes due to varied loads. Soft tissue thickness measurements were obtained from MRI data and were related to changes in blood flow. Additionally, normal and shear forces were applied to the forearms of individuals, and changes in skin perfusion were monitored as a function of temperature with three loading conditions.

The significance of the research conducted for this dissertation is that we are able to better understand the role that shear force plays with regard to blood flow and deformation. Both blood flow and deformation have been linked to tissue necrosis. Further, the permeability approach developed and demonstrated in this research will be useful to further explore body segment regions that are susceptible to tissue necrosis and pressure ulcer initiation under given loads. The studies between blood flow and soft tissue thickness, and blood flow and skin temperature provide insights with regard to the role these factors may play in pressure ulcer formation. Through this knowledge, improved ulcer prevention methods can be developed, ultimately leading to a reduction in the prevalence of pressure ulcers.

2. QUANTIFYING THE EFFECTS OF EXTERNAL SHEAR LOADS ON ARTERIAL AND VENOUS BLOOD FLOW: IMPLICATIONS FOR PRESSURE ULCER DEVELOPMENT

(Manorama A, Meyer R, Wiseman R, Bush TR. Quantifying the effects of external shear loads on arterial and venous blood flow: Implications for pressure ulcer development. Clinical Biomechanics 28, 2013, 574-578)

2.1 Introduction

Forces applied to the skin cause a decrease in regional blood flow. This decrease in blood flow can cause tissue necrosis and lead to the formation of deep, penetrating wounds called pressure ulcers (Kosiak, 1961; Zhang and Roberts, 1993). These wounds are detrimental to individuals with compromised health, such as the elderly and spinal-cord injured, and can lead to lengthy recovery periods and even mortality (Olesen et al., 2010). In addition, pressure ulcers have also been observed in immobilized neonates and children. Although the effects of pressure (normal load) on tissues have been studied, a person rarely experiences normal load alone, but rather a combination of normal and shear loads, particularly when seated or lying on an inclined bed (Bush and Hubbard, 2007; Mimura et al., 2009).

Pressure ulcers are a considerable health concern not only in the United States, but globally. In 2006, pressure ulcers were noted in over a half million hospital stays in the United States, which was a 79% increase from 1993, and 12% of pressure ulcer related hospitalizations resulted in mortality. Pressure ulcer incidence has been found to be in between 4 and 10% of patients admitted to acute hospitals in the United Kingdom (Clark et al., 2004). The average district general hospital's cost of pressure ulcers in the United Kingdom has been estimated to be in the region of £600,000 - £3 million per year (NHS Institute for Innovation and Improvement, 2009).

More than 90% of pressure ulcer related hospitalizations in adults were for treatment of other co-morbidities such as septicemia, pneumonia and urinary tract infection (Russo et al., 2008). Additionally, nearly three out of four patients diagnosed with a pressure ulcer were 65 years and older (Russo et al., 2008). Among the older population, over 50% of the individuals who were bedridden or wheelchair-bound developed pressure ulcers (Bansal et al., 2005; Sugarman, 1985). Among the younger adults hospitalized for pressure ulcers, paralysis and spinal cord injury were the common co-existing conditions (Russo et al., 2008). Pressure ulcers have been reported in pediatric population too. In pediatric intensive care units, prevalence rates have been as high as 27%, and in neonatal intensive care units, rates as high as 23% have been reported (Baharestani and Ratliff, 2007). Additionally, the recurrence rates of pressure ulcers have been reported to be as high as 39% (Keys et al., 2010) indicating that current preventive measures have not been highly successful.

Pressure ulcers are most likely to develop in areas of the body where the dermal tissues are subject to sustained mechanical loading between bony regions and an external structure such as a wheelchair or mattress. The National Pressure Ulcer Advisory Panel (NPUAP) and the European Pressure Ulcer Advisory Panel (EPUAP) highlight pressure as an important extrinsic factor in pressure ulcer development (EPUAP, 2009; NPUAP, 2009). It has been found that pressure on the skin, with time, causes an occlusion of blood flow, leading to obstruction of the transport of nutrients like oxygen to the cells, and also the transport of waste products away from the cells (Goossens et al., 1994; Kosiak et al., 1958; Bansal et al., 2005, Bouten et al., 2003). This results in necrosis (death) of the skin and underlying tissues and pressure ulcers are the result of such tissue damage (Bouten et al., 2003).

It is unclear if pressure ulcers start at the skin level and proceed inwards toward the muscle, or if they start at the muscular level and later propagate to the dermal and epidermal regions. Research has confirmed that pressure causes a reduction in perfusion of the skin and the addition of shear force reduces the perfusion further (Bennett et al., 1979; Manorama et al., 2010; Zhang and Roberts, 1994, 1993). However, few studies have explored the changes of arterial and venous blood flow with the addition of shear loads in humans. By coupling research on how loading affects blood flow in the larger vessels and how perfusion in the skin is affected with applied loads, a better understanding of the mode of pressure ulcer propagation can be developed.

Thus, the purpose of this research was to quantify the effects of different loading conditions, in particular, combined loading, on blood flow in arteries and veins of the forearm through the use of magnetic resonance angiography (MRA) phase-contrast imaging. As a result of this work, insights can be garnered with regard to where tissue damage is likely to occur, and will lead to a better understanding of how pressure ulcers propagate.

2.2 Methods

2.2.1 Subjects

Fifteen males voluntarily participated in this study which was approved by Michigan State University's Biomedical and Health Institutional Review Board (IRB# 10-1304). In addition to signing a consent form to participate in the research, all individuals completed a health questionnaire to confirm they were not under any medical care, not claustrophobic and did not have any internally implanted devices that could interact with the magnetic resonance imaging (MRI) scanner.

2.2.2 Equipment

The equipment used for this study included a MRI scanner, MRI coil, blood pressure cuff, rapid cuff inflator and air source, heart rate monitor, and shear load application system. The MRI scanner was a 3.0 T scanner by General Electric Healthcare systems (Fairfield, CT, USA). The scanner consisted of a bore into which the subject was positioned in a prone position (Figure 2-1). To improve the image resolution, a MRI coil was placed inside the scanner in such a way that the subject lying down in prone position on the scanner bed had his forearm inside the coil.

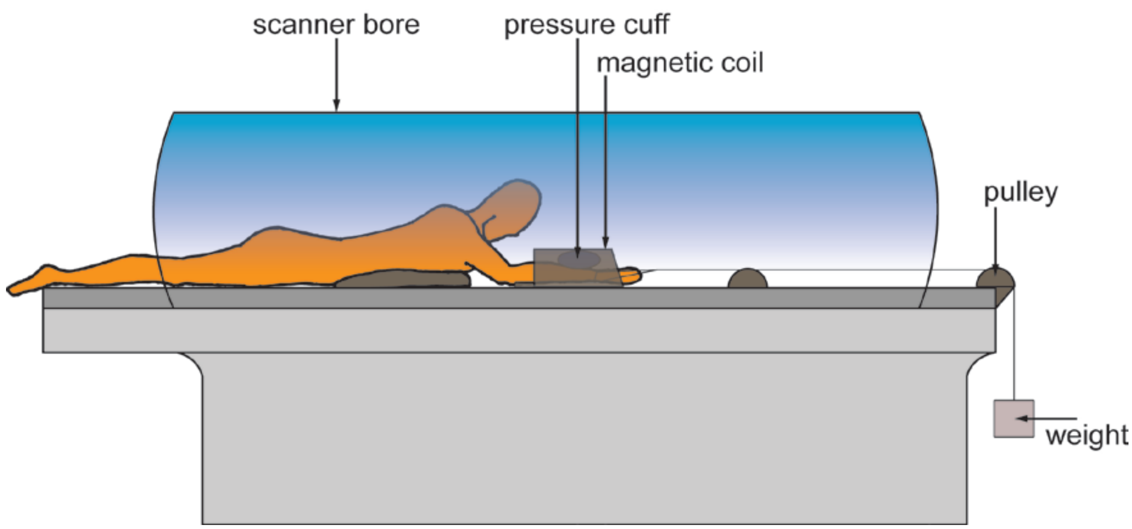

Figure 2-1: Experimental setup showing application of loads inside a MRI scanner. For interpretation of the references to color in this and all other figures, the reader is referred to the electronic version of this dissertation.

A blood pressure cuff (Dura-cuf REF 2779) by Johnson & Johnson (New Brunswick, NJ, USA) was used to apply normal loads on the forearm. The cuff was folded and placed between the arm and the coil, so that when inflated, it produced a normal load on the top of the forearm (Fig. 1). An inflator (E20 Rapid Cuff Inflator, Hokanson Inc., Bellevue, WA, USA) was used in conjunction with an air source (AG101, Hokanson Inc., Bellevue, WA, USA) to inflate the vascular cuff. The inflator system was located outside the MRI suite, with the tubing for the air connecting to the cuff inside the MRI suite.

To apply the shear load to the skin, a one-inch wide webbing (Keeper, Hampton Corporation, Foothill Ranch, CA, USA) was snugly wrapped around the forearm and secured with Velcro. On two sides of the webbing, a small rope was connected, so that when loading was applied to the rope, the friction between the webbing and skin applied a shear load uniformly to the skin (Figure 2-2). The application of the load to the webbing was through a pulley-weight system designed and constructed of materials that were appropriate for the MRI setting (i.e. non-conducting, non-metallic, and non-magnetic). The webbing applied loading to the skin such that the arm did not move, but the skin and tissues sheared relative to the bone.

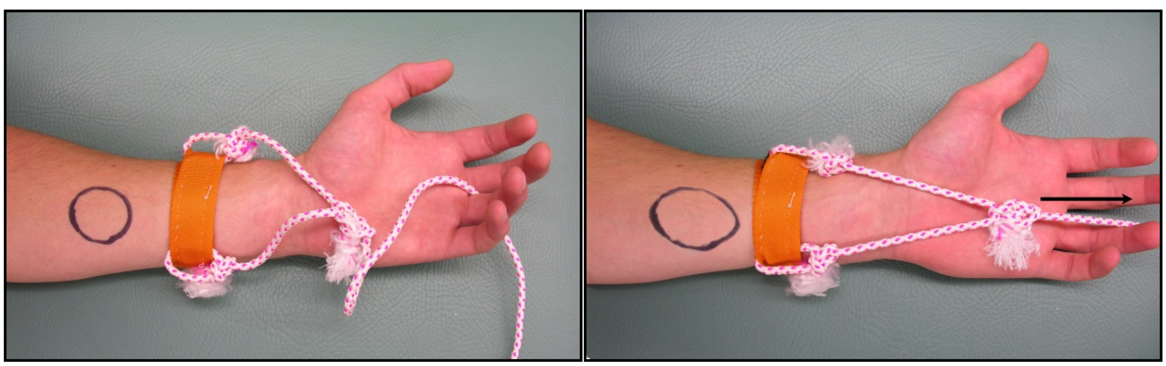

Figure 2-2: Figure showing the application of shear force through the friction created between the webbing and skin

The forearm was selected as the test site because of accessibility, and because of the coils available for the study. The size of the coils limited testing to either the arm or the leg. Pressure ulcers occur in the forearm, although the forearm is not listed as the site with the highest incidence of ulcers (Brillhart, 2005; Fujioka et al., 2010).

2.2.3 Experimental protocol

After consenting to participate, the individual was escorted into the MRI suite, and was assisted onto the MRI bed and asked to lie in a prone position. Pillows were positioned under the chest and head of the participant for comfort. The participant's right forearm was placed inside the coil. Two small support cushions were used to support the wrist and elbow on either end of the coil, so there were no lips or ledges that could produce areas of high load. The blood pressure cuff was placed inside the MRI coil, between the coil and the top of the forearm, at the midpoint of the length of the coil. The cuff was connected to the inflator system, located in the operator's room and the heart rate monitor was clipped on to the participant's right index finger in order to synchronize the blood flow measurements with the participant's heartbeat.

Each test session lasted for approximately 30 minutes. After arranging the experimental setup as described in the previous section, the participant was moved into the MRI scanner, using the motorized scanner bed. Once the subject was in the scanner, the test protocol began and the participant was advised to remain still for the remainder of testing. Each individual participated in three test conditions - baseline, normal load, and normal plus shear loads. Baseline was the first condition, and the order of the other two conditions was alternated across participants. The second and the third conditions were separated by a resting time of five minutes where no loads were applied to the arm.

For the baseline condition, no loads were applied on the forearm, and the blood flow data were collected using MRA phase contrast imaging. For the normal load condition, the pressure cuff was inflated to a pressure of 20 mm Hg, and the angiography data were again collected, after which the cuff was deflated and a resting period occurred. For the combined load condition, the pressure cuff was inflated to a pressure of 20 mm Hg and following the application of this load, a shear load was applied using the pulley-weight system. The weight in Figure 2-1 was 20N. Again, angiography data were recorded. Since the image samples were based on the cardiac cycle of the individual, the time of each test varied slightly ranging from 47 to 112 seconds. Additionally, the magnitude of applied loads were chosen based on previous studies (Bush and Hubbard, 2007; Manorama et al., 2010).

After the three conditions were conducted, a time-of-flight (TOF) scan was performed. The TOF scan yielded a 3D representation of the blood vessels in the scanned region. The TOF scan lasted five minutes, after which the participant was moved out of the scanner. The purpose of the TOF scan was to help locate the blood vessels in the cross-sectional slices during the segmentation part of the analysis process.

The final step of this experimental procedure involved determining the contact area of the pressure cuff on the forearm so that the pressure applied in the normal condition could be converted to an equivalent load in Newtons. Therefore, the contact area was measured so that the force could be calculated as the ratio of pressure over area. For this purpose, the participant was asked to sit on a chair and place his forearm inside a replica of the magnetic coil. The pressure cuff was folded in the same way as it was for the test conditions, and the lower surface of the cuff was dyed with a washable, acid-free and non-toxic dye (Adirondack Pigment Ink, Ranger Industries Inc., Tinton Falls, NJ). The pressure cuff was placed into the coil over the forearm, and inflated. When it inflated, the contact between the skin and the cuff left an inked marking on the skin, identifying the contact area. In all participants, the marking was a trapezoidal shape. The sides of the trapezoid were measured with a flexible tape measure and the contact area computed. This contact area was used to calculate the normal force for each participant. Finally, the dye was removed from the participant's forearm; and the individual was paid for participating in the study. This marked the end of the test session.

2.2.4 Magnetic Resonance Angiography

The study employed the principle of Magnetic Resonance Angiography (MRA) to measure the blood flow in the vessels of the forearm. MRA is a set of techniques based on Magnetic Resonance Velocimetry and uses the sensitivity of blood flow to magnetic resonance to obtain anatomical images of the blood vessels. MRA involves separating signals produced by flowing materials from signals produced by static material in the body. Specifically, the approach of phase contrast magnetic resonance imaging (PC-MRI) was used for this research and has been validated by other researchers (Elkins and Alley, 2007; Meyer et al., 1993; Radda et al., 1981).

2.2.5 Data Analysis

(i) Determining the volumetric flow rate

From the experiments, MRA images (Figure 2-3) were obtained for the cross section of the forearm. Four slices were recorded for each test condition; each slice was 3 mm thick, and consecutive slices were spaced at a distance of 5 mm from one another. For each slice, blood flow data corresponding to 20 time points in the phase of a cardiac cycle were measured; and for each time point, there was a velocity image and a magnitude image. The velocity image contained the blood flow velocity data, while the magnitude image contained the anatomical structures, including the boundaries of the vessels and other tissues.

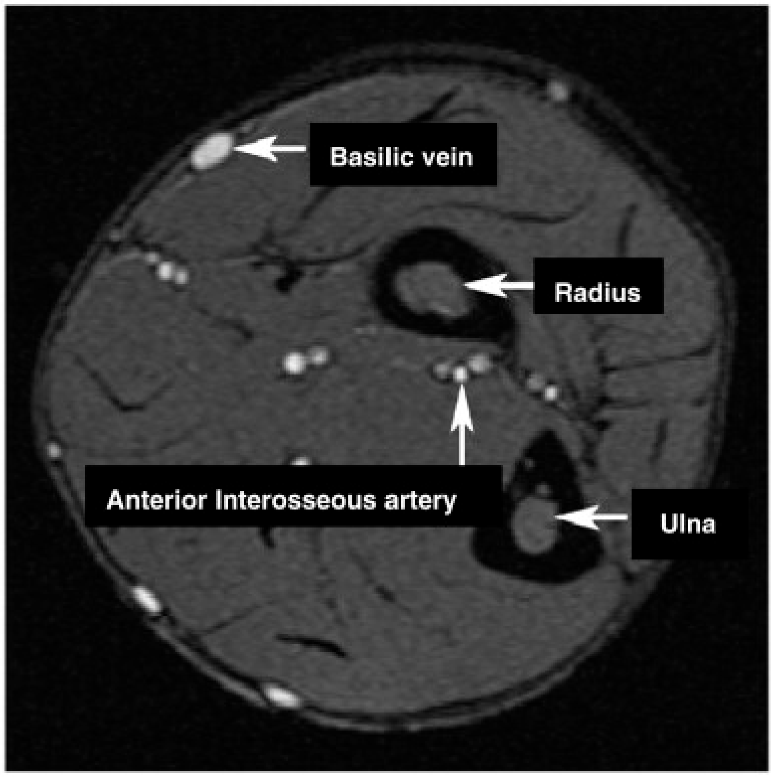

Figure 2-3: Single cross sectional MRA image. Vessels are shown as white regions due to flowing material.

The blood flow rates were computed in two blood vessels of the forearm- anterior interosseous artery (AIOA), and basilic vein (BV). These two vessels were selected because they were visible in the images from all participants. The areas corresponding to these vessels were selected using Winvessel, a segmentation software (Michigan State University, East Lansing, MI), (Meyer et al., 1993). During segmentation, a variable Region of Interest (ROI) tool was used to manually select the boundaries of the AIOA and BV in the magnitude images. Once each area was selected, the ROI was used to find the corresponding velocity in that area from the velocity images. Next, a zero correction (zero velocity value) was acquired from the velocity image. The zero velocity value was obtained by selecting a square ROI in a region corresponding to no blood flow in the MRA image. A zero velocity value was recorded for each condition and was subtracted from the measured velocities, resulting in the actual velocities of blood flow. This procedure produced the velocities of blood flow in each time point in all four slices for all three loading conditions. Also, the areas of the blood vessels at each slice were measured from the software. Using these data, the volumetric flow rate ($q_{n,t}$) for each slice at each time point was determined using the following formula:

$$q_{n,t} = v_{n,t} A_n$$

where n is slice number (1-4); t is time point (1-20); $v_{n,t}$ is blood flow velocity (mm/s); A_n is area of cross section of blood vessel (mm^3); and $q_{n,t}$ is volumetric blood flow rate (mm^3/s).

The blood flow rates were averaged across all 4 slices. These values were further averaged across the 20 time points, thus providing an average blood flow rate value (Q) for each loading condition. In other words, the final blood flow rate for each blood vessel was determined using the following formula:

$$Q = \frac{1}{80}\left(\sum_{t=1}^{20}\sum_{n=1}^{4} q_{n,t}\right)$$

(ii) Statistical analyses

The blood flow rates in each loading condition were compared statistically for differences, using one way repeated measures ANOVA. The statistical analyses were two-tailed, and were performed at a confidence interval (CI) of 90%. A 90% CI was used instead of the conventional 95% owing to the small sample size of the study (Huberty, 1987; Labovitz, 1968). In addition to tests of statistical significance, effect sizes were calculated for each comparison.

2.3 Results

2.3.1 Participants

Participants ranged in age from 18 to 44 years (Ave. 26, SD 8). Participants' masses ranged from 59 to 105 kg (Ave. 74, SD 11). Fourteen out of fifteen participants had a BMI of less than 30, where a score of more than 30 denotes obesity, according to the Centers for Disease Control and Prevention. One participant had a BMI of 35. All individuals were in good health and not currently under the care of a physician for any issues.

2.3.2 Applied normal loads

The contact area of the pressure cuff with the top of the forearm when normal loads were applied ranged from 0.004 to 0.009 m^2, with an average of 0.006 m^2. A pressure of 20 mm Hg when applied over these calculated contact areas resulted in an average normal force of 17 N across the subject pool.

Table 2-1: Effect size of statistical comparisons of blood flow at various loads (Q is average blood flow rate)

	Anterior interosseous artery		Basilic vein	
Comparison	**Difference in Q (mm^3/s)**	**Effect size**	**Difference in Q (mm^3/s)**	**Effect size**
Baseline & Normal	3.24	0.40	133.23	0.33
Normal & Normal+Shear	3.26	0.32	56.83	0.46
Baseline & Normal+Shear	6.50	0.49	190.05	0.49

2.3.3 Volumetric blood flow rates

A decreasing blood flow trend was observed with the highest flow occurring in the baseline condition and the lowest in the combined load condition, suggesting that blood flow in the AIOA and BV decreased further with the addition of shear as compared to normal load alone (Figure 2-4). When the blood flow rates were statistically compared between the three loading conditions, a statistically significant difference ($p=0.08$) was found for the comparison involving the AIOA. The comparison involving the BV yielded a marginally significant p-value of 0.10.

Medium to high effect sizes were observed for the comparisons involving both the vessels (Cohen, 1988). Effect sizes ranged from 0.3 to 0.5 (Table 2-1). This suggested that the marginal significance was not due to the absence of an effect, but was due to the small sample size of 15.

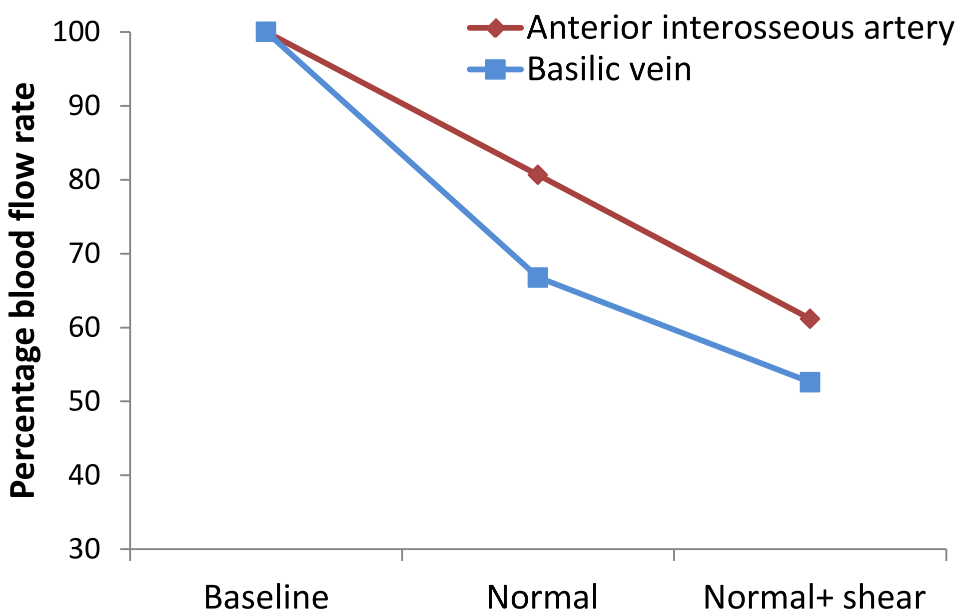

Figure 2-4: Decreasing blood flow rates with application of normal and shear loads.

2.4 Discussion and Conclusions

The goal of this research was to study the changes in the arterial and venous blood flow in the forearm through the use of MRA phase-contrast imaging with the application of normal and shear loads.

The results of the experiments demonstrated that with the addition of shear loads, blood flow in the AIOA and BV decreased further than with the addition of normal load alone. While the AIOA comparisons produced significant differences, only a marginal significance was observed in the case of BV. However medium to high effect sizes were observed, suggesting that the marginal significance was due to the small sample size and statistical significance could be obtained with a larger sample.

Published research has indicated that when sitting, or lying in an inclined bed, an individual experiences both normal and shear loads on the body (Bush and Hubbard, 2007; Gilsdorf et al., 1990; Goossens et al., 1997; Hobson, 1992; Mimura et al., 2009). A limited number of studies have examined the effects of shear loading on the skin in humans. Those studies reported that the transcutaneous blood flow decreased with the addition of shear applied to the skin (Bennett et al., 1979; Manorama et al., 2010; Zhang and Roberts, 1994, 1993). However, until now, it was not clear what effect an external shear load had on deeper vessel blood flow. The work presented here confirms that external loads of combined normal and shear forces decrease the internal blood flow, more so than normal load alone.

This research was novel on two levels. First, the methods were unique in that shear and normal loading were applied while in an MRI scanner. An apparatus was developed to consistently apply both normal and shear loads to the forearm while meeting all the requirements for use in the MRI scanner. Secondly, the use of MRA phase-contrast imaging in combination with *in vivo* shear loading on humans to document changes in blood flow is novel. Scientific literature reporting such results is not available elsewhere.

Results also indicated that a variation in normal force occurred across the subject pool. This was due to the anatomical build of the individual, and how the pressure cuff interacted with the individual's forearm. However, in the data analysis, each data set was compared to the individual's own baseline data, so analyses were conducted on the change in blood flow from the baseline values per each individual. A limitation of this study was that the shear loads at the site of the study (MRI suite) could not be measured. So, it is possible that some variation in shear loading occurred across participants. Additionally, another limitation is that this study involved only male participants, whereas women are also prone to pressure ulcers. Future work will include female participants.

Based on the results of this work, shear loads applied at the skin cause a reduction in blood flow in the deeper vessels. From prior work of the authors, (Manorama et al., 2010), it was found that the perfusion at the skin level decreased with the addition of shear loads. The current data in conjuction with this prior study shows that a decrease in blood flow occurs at both the superficial and deep levels when shear loading is applied on the skin. Additionally, research shows that a decrease in blood flow leads to tissue necrosis (Bansal et al., 2005; Bouten et al., 2003; Goossens et al., 1994; Kosiak et al., 1958). Thus, based on this information, both scenarios of pressure ulcer formation are possible, i.e. pressure ulcers could be initiated superficially, or at a deep level. Future research will combine the understanding of the effects of shear load on superficial perfusion and on deeper vessel blood flow though a porous media model to obtain a better understanding of where a pressure ulcer is likely to be initiated.

The findings from this work indicate that shear force is an important factor to consider when studying the changes in blood flow. Additionally because of the relationship between decreased blood flow and tissue damage, understanding the effects of shear in the formation, prevention, and treatment of pressure ulcers should also be considered.

3. UNDERSTANDING THE EFFECTS OF NORMAL AND SHEAR FORCES IN RELATION TO PRESSURE ULCERS: A SUBJECT-SPECIFIC 3D MODEL OF THE HUMAN FOREARM

3.1 Introduction

The National Pressure Ulcer Advisory Panel (NPUAP) and the European Pressure Ulcer Advisory Panel (EPUAP) have indicated the severe nature of pressure ulcer (PU) development for both young and older adults (EPUAP, 2009; NPUAP, 2009). PUs are a considerable health concern, and have been documented in over a half million hospital stays in the United States. In the United Kingdom, up to 32% of hospital patients, and up to 21% of people in nursing homes were affected by PUs (Kaltenthaler et al., 2001). Over 75% of patients diagnosed with a PUs were 65 years and older (Russo et al., 2008). Among this older population, over 50% of the individuals who were bedridden or wheelchair-bound developed PUs (Bansal et al., 2005; Sugarman, 1985). Among the younger group, PUs have been observed in pediatric and neonate population, younger adults with paralysis and spinal cord injury, and individuals who wear prosthetic devices (Baharestani et al., 2009; Curley et al., 2003; McLane et al., 2004; Portnoy et al., 2009; Russo et al., 2008; Whitney et al., 2006).

There are conflicting theories on where PUs initiate. It is unclear if they start at the skin level and proceed inwards toward the muscle, or if they start at the muscular level and later propagate to the dermal and epidermal regions (Agam and Gefen, 2007; Shea, 1975; Versluysen, 1986) .

Additionally, there are two schools of thought with regard to how loading and tissue necrosis are related (Olesen et al., 2010). First, and most widely accepted, is that forces on the skin cause an occlusion of blood flow, leading to obstruction of the transport of nutrients like oxygen to the cells, and also the transport of waste products away from the cells (Bouten et al., 2003; Brooks, 1922; Goossens et al., 1994; Kosiak, 1959; Kosiak et al., 1958). This results in necrosis of the skin and underlying tissues, thus initiating a PU (Bouten et al., 2003). The other theory is that loading on the skin results in tissue deformation, which, independent of blood flow, causes individual cell death and leads to a PU (Breuls et al., 2003; Gawlitta et al., 2007a).

Although research has been published on PUs, most of this work focuses on normal loading, and does not include shear forces (Bansal et al., 2005; Parish and Witkowski, 2004). In fact, in the typical seated or bed environments (e.g. lying on an inclined bed or seated in a wheelchair), shear forces are present (Bush and Hubbard, 2007; Mimura et al., 2009; Reuler and Cooney, 1981). Among the few studies that evaluated aspects of shear forces, most are from animal evaluations (Goldstein and Sanders, 1998; Linder-Ganz and Gefen, 2007a). Few researchers have explored the effects of shear loading in humans (Goossens et al., 1997; Manorama et al., 2013, 2010) and none have conducted anatomically representative modeling to explore the effects of external shear forces on mechanical factors such as internal stress, strain and deformation in humans.

Also, limited modeling work has been conducted around PU formation. Researchers have developed simplified representations of the body and evaluated the effects of normal load on a region (Chow and Odell, 1978; Gefen, 2007; Reddy et al., 1980). For example, Gefen developed a model of the buttocks, in which the ischial tuberosity was represented by a rigid half-sphere, and the gluteus muscle was represented by an elastic half-space (Gefen, 2007). Other researchers have developed anatomically accurate finite element (FE) models of the buttocks to study the effects of externally applied normal forces on internal stresses (Linder-Ganz et al., 2007; Makhsous et al., 2007; Sun et al., 2005). These models have been successful in obtaining the internal stress distributions due to externally applied normal loads. However, the application of external shear load in addition to normal load and its effects on internal stresses and deformation in the skin and muscle tissue with an anatomically representative model is absent from the literature.

To determine if tissue necrosis is caused by blood occlusion, deformation, or both, and to better understand the location of tissue damage initiation, experimental studies alone will not suffice; they must be combined with anatomically accurate FE models. In particular, the need to study a realistic loading environment, one that includes shear forces, exists.

Thus, the objective of this research was to develop an anatomically accurate 3D FE model of the forearm to study the effects of externally applied normal and shear loads on internal stresses and deformation and to relate the deformation results to experimental data. The forearm was selected because of availability of prior data for this anatomical region (Manorama et al., 2010), and it is a site for PU formation (Brillhart, 2005; Fujioka et al., 2010).

The results of the model, in combination with experimental studies relating the effects of normal and shear forces on blood flow, are crucial to the understanding of the mode and direction of PU initiation and propagation.

3.2 Methods

3.2.1 Overview

The study presented in this paper is of a subject-specific FE model of a forearm section. This 3D model was constructed from 2D MRI slices obtained during an experiment to study the effects of normal and combined loads on blood flow. The details of the experimental study are described, followed by the modeling procedure.

3.2.2 Participant

All research methods were approved by the University's Biomedical Institutional Review Board. The individual provided consent prior to participation. The subject-specific FE model was created from experimental data corresponding to a healthy male (age: 25 years). The participant had a mass of 68 kg with a height of 178 cm, and no vascular issues.

3.2.3 Experiment

To gather image data for the model, Magnetic Resonance Angiography (MRA), and Time-of-Flight (TOF) scans were obtained of the forearm. The purpose of the TOF scan was to obtain anatomically correct representations of the structures in the forearm, which were used to create the 3D model. MRA scans were recorded to obtain changes in blood flow in three loading conditions—baseline, normal, and normal plus shear load. These scans also provided changes in the overall deformation due to loading and were used to compare the results of the FE model with the experimental results.

The participant was asked to lie in a prone position inside a MRI scanner, with the right forearm placed inside a MRI coil (Manorama et al., 2013). The first condition was baseline, where no loads were applied, whereas for the second condition, an inflatable bladder was used to apply a normal load of 20 mm Hg (2.67 kPa) over an area of 82 cm^2. In the combined loading condition, a shear force of 15.6 N was applied on the skin of the forearm of the participant, in addition to the normal load. MRA scans were taken for all three conditions, while the TOF scan was taken with no loading on the forearm. A more detailed explanation of the MRI and MRA protocol is described in Chapter 2 of the dissertation.

3.2.4 MR image specifications

The MR scans were performed in a 3T MR scanner (GE Healthcare, Little Chalfont, UK). The images were 256 x 256 pixels, with a field of view of 10 x 10 cm. The TOF scan delivered 52 cross-sectional image slices of the forearm section, corresponding to the baseline condition. The inter-slice thickness was 0.2 cm.

The angiographs contained four cross-sectional slices for each of the three loading conditions. Each slice was 0.3 cm thick, and consecutive slices were spaced at 0.5 cm from each other. For each slice, blood flow data corresponding to 20 time points in the phase of a cardiac cycle were measured; and for each time point, there was a velocity image and a magnitude image. The magnitude image was of relevance to this study, as it contained the anatomical structures, including the boundaries of the vessels and other tissues for the loaded conditions.

3.2.5 Model construction

Each of the slices from the TOF scans were imported into parallel work-planes spaced at a distance of 2 mm from each other, in Autodesk Inventor (Autodesk Inc., CA). On each of these cross sectional slices, the structure of the two forearm bones (radius and ulna), muscle, skin, anterior interosseous artery (AIOA), and basilic vein (BV) were segmented. After segmentation, the structures were lofted from one slice to the next, creating the 3D model (Figure 3-1). Next, a section corresponding to the pressure application area, was created on the skin surface of the model.

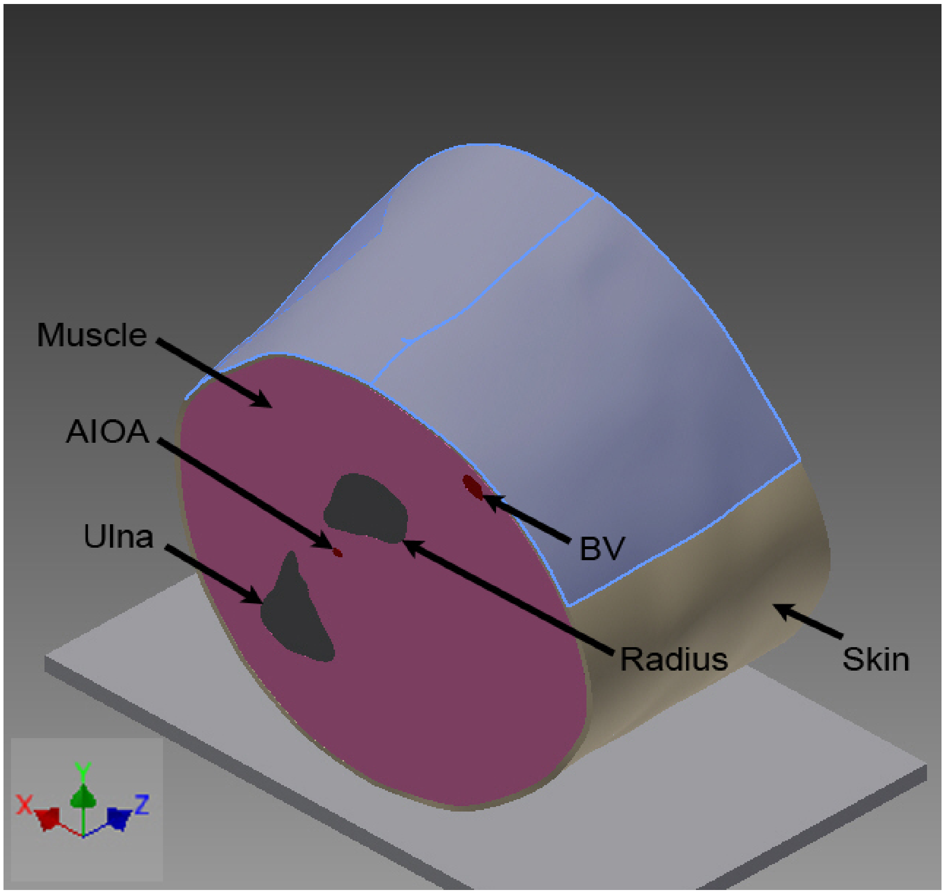

Figure 3-1: 3-D model of forearm section. The radius, ulna, anterior interosseous artery (AIOA), basilic vein (BV), muscle, and skin can be seen. The cut section of the skin represents the area to which normal loads were applied.

The model, comprising of the bones, muscle, skin, and ground surface, was meshed in Autodesk Simulation Multiphysics (Autodesk Inc., CA), using a mix of 157144 brick and tetrahedral elements.

3.2.6 Material properties

The material properties, including mass density, Young's modulus, and Poisson's ratio for the skin, muscle, and bone were obtained from literature (Agache et al., 1980; Balar et al., 1989; Chabanas and Payan, 2000; Fung, 1993; Nordez and Hug, 2010; Pailler-Mattei et al., 2008;

Zadpoor, 2006) (Table 3-1). Elastic isotropic properties were assumed for all materials. The ground surface, representing the MRI table, was considered to be a rigid surface.

Table 3-1: List of material properties used in the FE model, (Agache et al., 1980; Balar et al., 1989; Chabanas and Payan, 2000; Fung, 1993; Nordez and Hug, 2010; Pailler-Mattei et al., 2008; Zadpoor, 2006).

Part	Mass density (kg/m^3)	Young's modulus (N/m^2)	Poisson's ratio
Bone	1900.0	1.72×10^{10}	0.30
Muscle	1041.0	1.10×10^{5}	0.49
Skin	1110.0	2.00×10^{7}	0.49
Ground	2404.5	2.07×10^{10}	0.15

3.2.7 Boundary conditions, loading conditions and analysis parameters

The ground surface was constrained in all directions. The outer surfaces of bones were constrained in the x and z axes, which represented the medio-lateral and proximal/distal directions respectively, but were left unconstrained in the vertical Y direction, to account for motion as the forearm contacted the ground surface.

A low-speed, frictionless, surface contact was defined between the skin surface and the ground to avoid penetration between the two surfaces. No-slip conditions were defined between the different interfaces such as bone-muscle, and skin-muscle, while making sure that the skin and muscle tissues could move axially during application of shear load.

Loads applied to the model matched those of the experiment and the analysis type was a Mechanical Event Simulation (MES) with non-linear material models. A standard gravity of 9.81 m/s^2 was applied in the vertical (Y) direction.

3.2.8 Experimental data used for model evaluation

The total deformations in 2D in the FE models were compared with those from experiments. The deformation obtained during the experiments was calculated as a measure of the forearm cross-sectional height at mid-plane (MH), and cross sectional width at mid-plane (MW) (Figure 3-2). These values were measured on the proximal slice of the MRA images. These deformation values were compared between the experiment and the model.

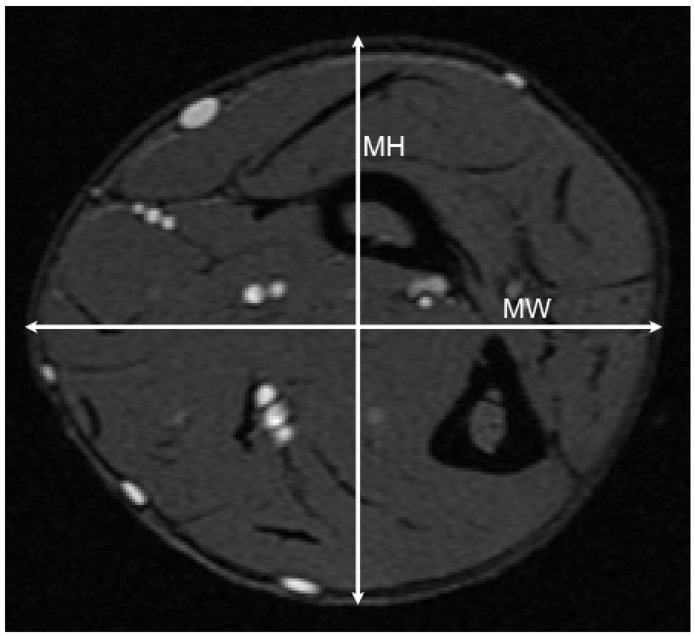

Figure 3-2: Phase Contrast-MRI magnitude image showing deformation measurements. Values from the MRI images for each of the three conditions were used for comparison with the model.

3.3 Results

Differences in stresses, strains, and displacements were found between the simulations of combined loads, in comparison to normal loads alone.

3.3.1 Stress

The maximum Von Mises stresses in the *muscle* were observed at the inferior side of the interface between muscle tissue and the ulna, in the distal end for the normal loading condition, and at the proximal end for the combined loading condition (Figure 3-3). Changes in stress patterns due to the addition of shear included stress concentrations at the muscle-bone interface, particularly at the ulnar interface along the length of the model. For the normal loading condition, the maximum Von Mises stress was 108 kPa in the muscle region, and it increased to 212 kPa for the combined loading condition.

Observation of individual stress tensors in the muscle region showed that the addition of shear changed the location of the maximum stresses in all three directions. In the normal loading condition, maximum values were observed at the ulnar interface, whereas in the combined loading condition, maximums were observed on the radial and ulnar interfaces. The stress patterns showed higher magnitudes around the bones, which spread further into across the muscle tissue, with the addition of shear. The ranges of magnitudes of the tensors were between -0.44 to 0.4 KPa for σ_{xx}, -0.44 to 0.3 KPa for σ_{yy}, and -0.41 to 3.1 KPa for σ_{zz}.

As for the *skin*, the locations of maximum Von-Mises stresses showed little variation with the addition of shear loads, and were observed at the skin surface touching the inferior side of the muscle, at the proximal end of the model. The addition of shear loads increased the maximum Von Mises stress from 368 kPa to 396 kPa.

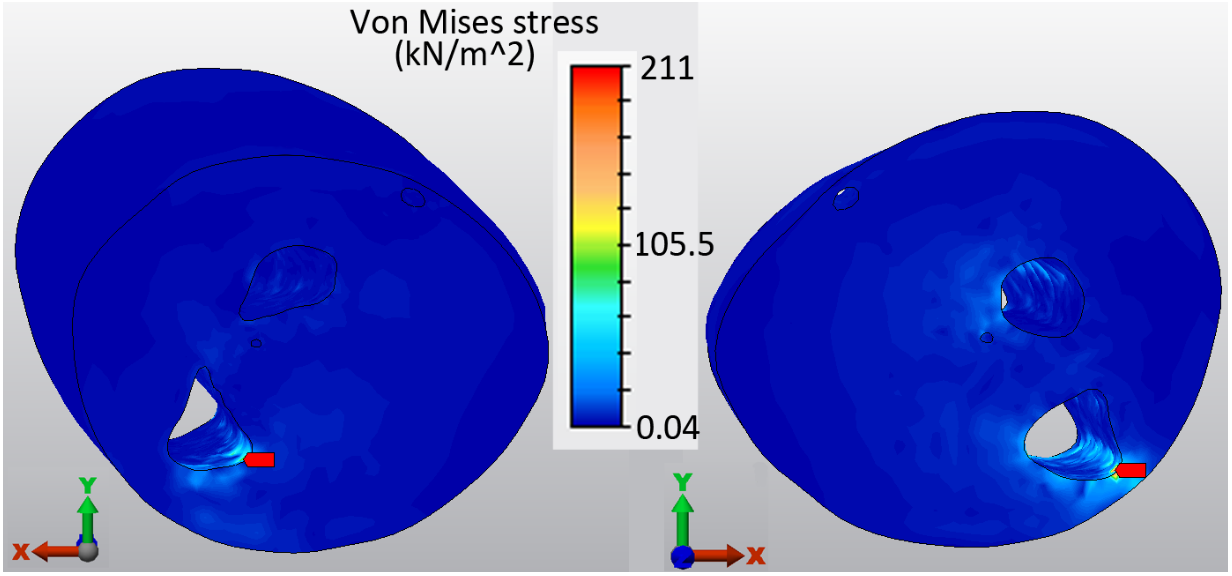

a)

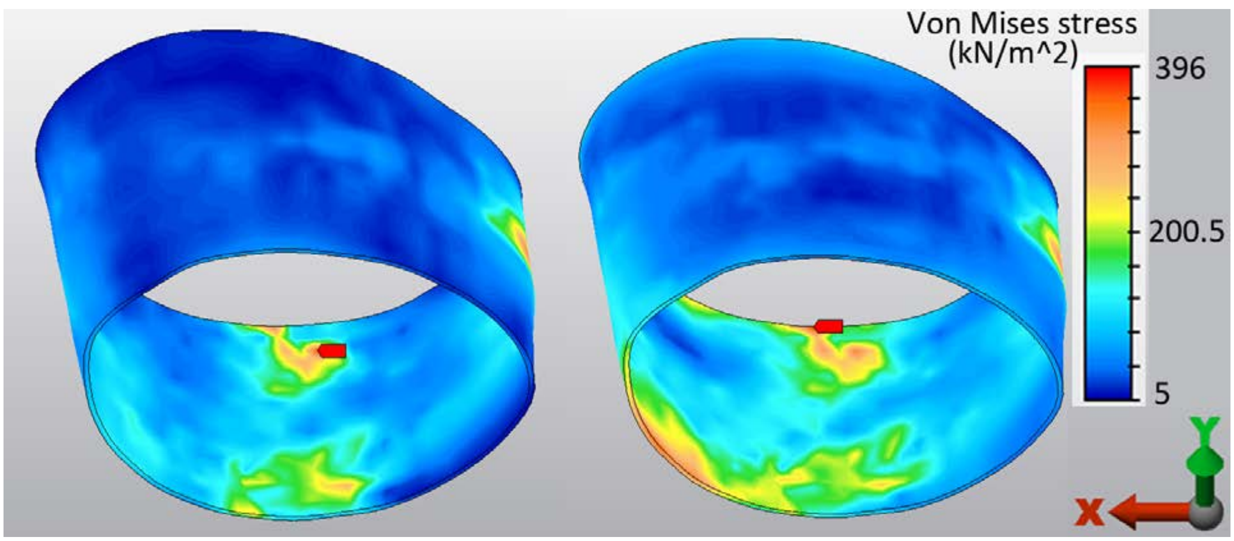

b)

Figure 3-3: Side-by-side comparison of Von Mises stress distribution due to normal and combined loading in a) Muscle tissues b) Skin tissues.

* Note in Figure a) the two views shown are different to show the location of maximum

* The stresses occur predominately around the bones (Bones are hidden in the model to allow for viewing of stress contours at the bone-muscle interface)

* The red marker shows the point of maximum displacement

For the skin tissues, the location of the maximum values of the individual tensor components did not change from normal to combined loading conditions. Maximum values were observed on the inferior side of the skin-muscle interface at the proximal end of the model and towards the distal end. There were no observable differences in the stress patterns between normal and combined loading. The ranges of tensor magnitudes were determined to be -5.2 to 6 KPa, -5.2 to 6. 2 KPa, and -5.2 to 6.2 KPa for σ_{xx}, σ_{yy}, and σ_{zz} respectively.

3.3.2 Strain and Deformation

The maximum strain in the *muscle* region was observed at the inferior ulnar-muscle interface at the distal end, in both the normal and combined loading conditions. The strain patterns showed a concentration around the radius when shear loads were applied. The maximum Von Mises strains increased from 0.2 in normal loading to 0.3 in combined loading condition. The skin region experienced maximum Von Mises strain in the inferior skin-muscle interface during the normal loading condition and in the distal end during the combined loading condition. The high strain regions were more wide-spread when combined loads were applied, and the maximum Von Mises strain showed an increase of 0.01 due to combined loads (Figure 3-4).

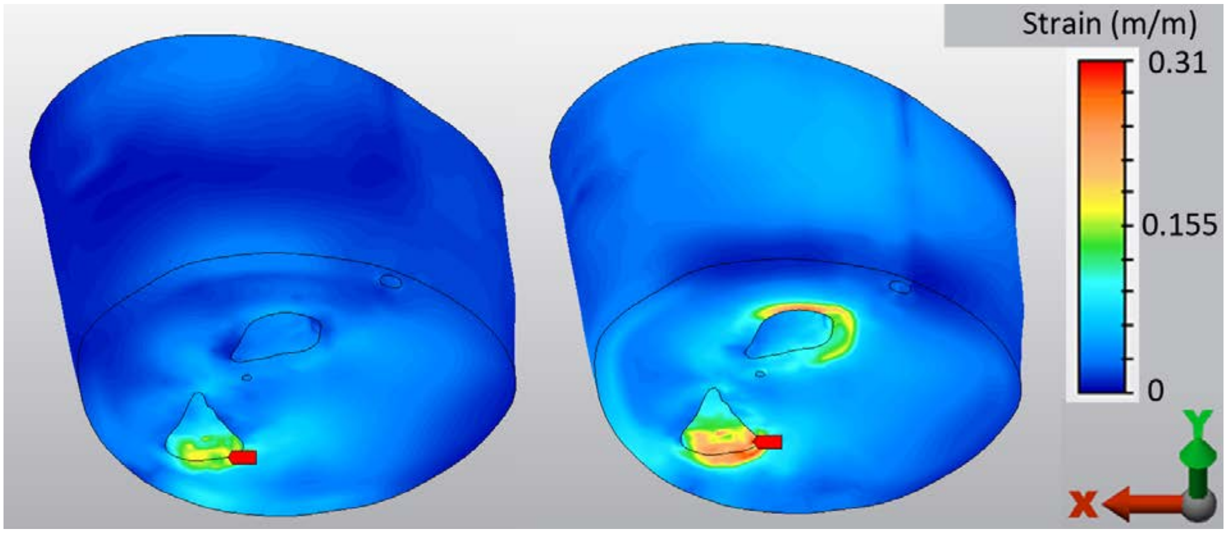

a)

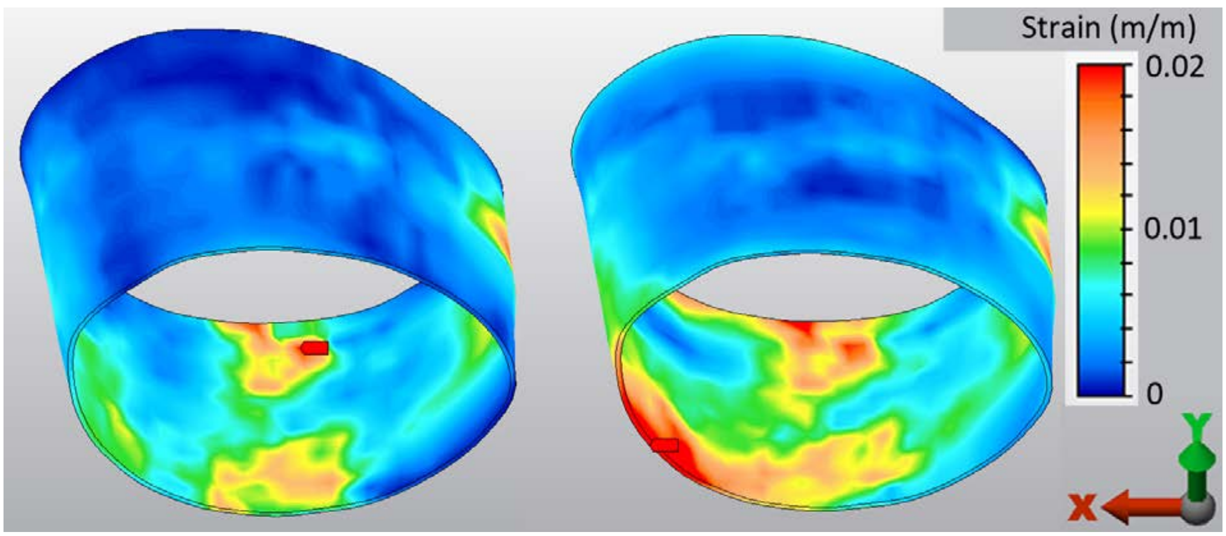

b)

Figure 3-4: Side-by-side comparison of Von Mises strains due to normal and combined loading in a) Muscle tisses b) Skin tissues.

* The red marker shows the point of maximum strain values

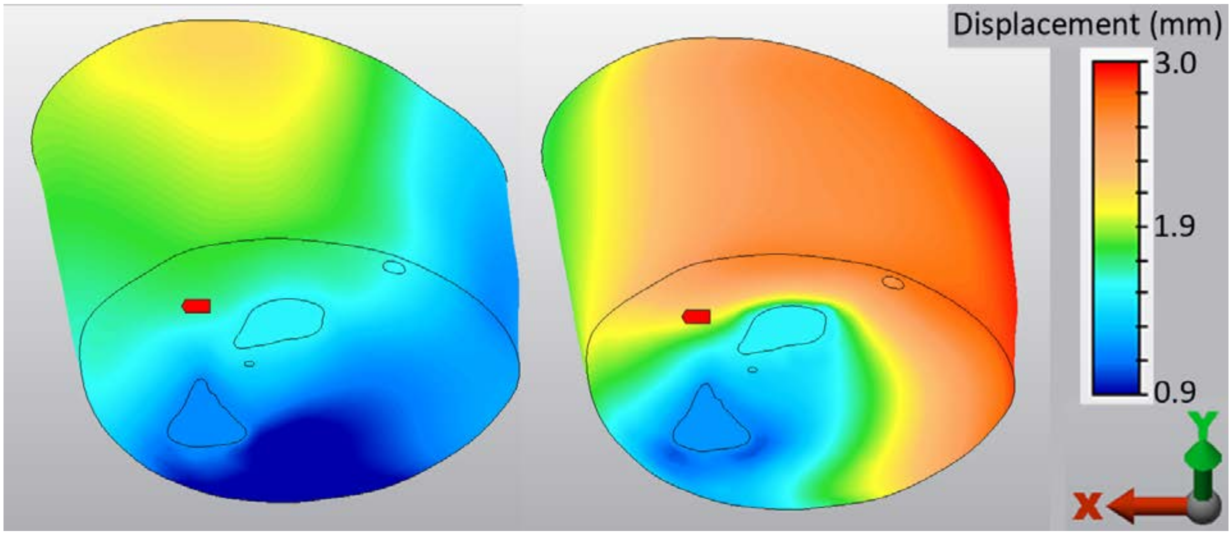

a)

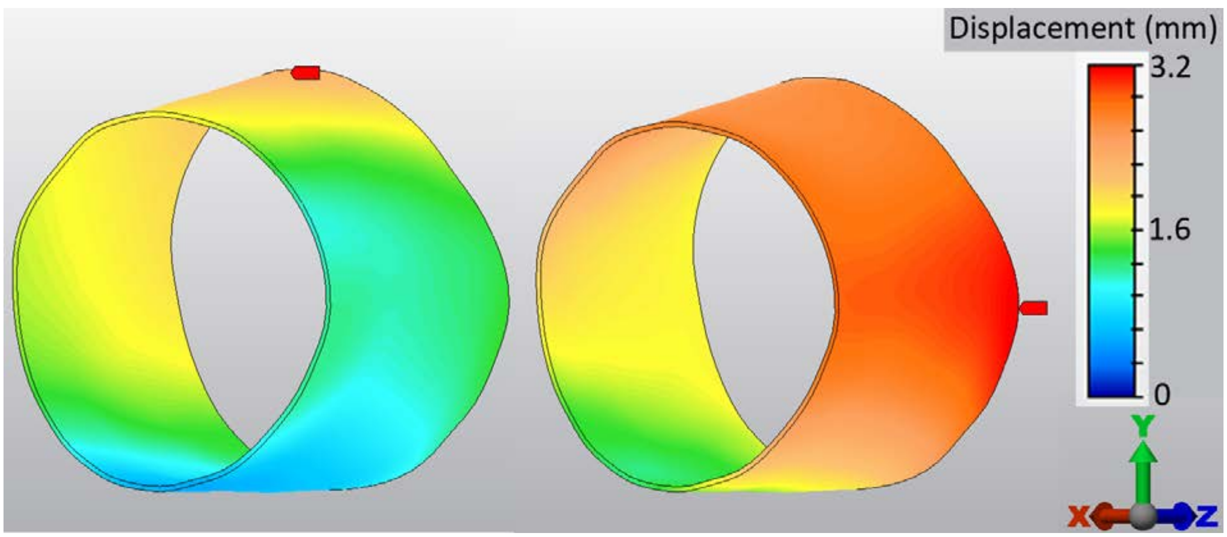

b)

Figure 3-5: Side-by-side comparison of resultant displacement due to normal and combined loading in a) Muscle tisses b) Skin tissues.

* The red marker shows the point of maximum displacement

* In muscle tissue, the maximum displacement is on the inner surface midway between the proximal and distal end

The resultant displacements were highest on the inner side of the model on the lateral half, for both normal and combined loading conditions (Figure 3-5). With the application of shear, the muscle tissues surrounding the bones experienced more displacement than those between the two bones. The maximum resultant displacement in muscle tissue was 16.2 mm for the normal loading condition, and 15.9 mm for combined loading condition.

As for the *skin* tissues, maximum resultant displacement values were observed on the superior side of the forearm, close to the proximal end for the normal loading condition. When shear loads were added, the maximum value shifted to the medial surface of the skin on the proximal end. The maximum resultant displacement increased from 2.2 mm to 3.2 mm due to the application of shear load.

3.3.3 Comparison with experimental data

The forearm cross sectional height at mid-plane (MH) and forearm cross sectional width at mid-plane (MW) for the model were compared with the experimental data.

The MH values from the experimental data showed a 1% decrease from baseline to normal loading condition, and a further 2% decrease from normal to combined loading condition. The MH values from the model showed a decrease of 2% from baseline to normal load condition, and remained same for the combined loading condition.

The MW values increased by 2% from baseline to normal loading condition, and remained the same through the combined loading condition, in both the experimental data and model.

3.4 Discussion and Conclusions

The objective of this study was to analyze the effects of normal and combined loads on the internal stresses and deformation of the skin and muscle tissues, using an anatomically accurate FE model of a forearm section.

The overall results of this study indicated that combined normal and shear forces caused increased stresses and strains in the skin and muscle when compared to normal forces alone. The maximum Von Mises stress in the muscle region nearly doubled due to the addition of shear forces. Skin tissues also showed an increase in Von Mises stresses due to shear, although not as large of an increase as the muscles. These results suggested that muscle tissues experienced a higher increase in stress than skin tissues but both were negatively impacted with the addition of shear load.

The location of maximum stresses and strains in the muscle region were at the bone-muscle interface, which was either the superior radial-muscle interface or the inferior ulnar-muscle interface. In the skin region, the maximum stresses and strains were found in the inferior forearm skin-muscle interface, although the increase due to shear loads were not as large as experienced by muscle tissues. Results also showed a clear relation between external shear and increased strain, for both skin and muscle.

The addition of shear loads increases the internal stresses, at the bone-muscle interface, which could be an initiation point for necrosis at the deeper level (Linder-Ganz and Gefen, 2007b). Skin stresses also increase due to external shear. This increase in skin stress supports that initiation of a PU could also be at the skin level. Thus, the results of this study suggest that ulcers could either initiate in the deeper muscle tissue and propagate superficially, or initiate at the skin level and propagate internally, supporting both of the proposed theories.

The previous work of the authors related the effects of combined loads to blood flow. This prior work identified a decrease in both the arterial and venous blood flow, as well as the superficial skin perfusion when shear loads were applied in addition to normal loads (Manorama et al., 2013, 2010). Some studies have suggested that although mechanical loading may be the direct cause of tissue damage, the associated ischemia could accelerate or amplify the damage, causing a PU (Gawlitta et al., 2007b; Stekelenburg et al., 2008). Thus, the results of this modeling study, combined with the prior work indicate that PU mechanism could be attributed to both ischemia and deformation.

The stress values of muscle and skin tissues obtained in this study were comparable with other studies (Linder-Ganz and Gefen, 2004; Oomens et al., 2003). Our study did not take into account the effect of time; however, previous literature suggests that a pressure of about 30 KPa applied for less than an hour could cause necrosis (Figure 3-6) (Linder-Ganz et al., 2006). It should be noted that these comparative studies were limited. The studies reported for comparison were conducted *in-vitro on* animal models, and shear forces were not included in these protocols. Similarly, the strain values obtained from our simulation were in the range of compressive strains that could lead to necrosis (Breuls et al., 2003; Gefen et al., 2008; Peeters et al., 2003). Breuls et al. indicated that compressive strains of 30-50% caused death of 50% of muscle cells within 6 hours. Gefen et al. suggested that cells could tolerate strains below 40% for up to 4.75 hours. It has also been suggested that strains exceeding 77% could cause instantaneous cell death.

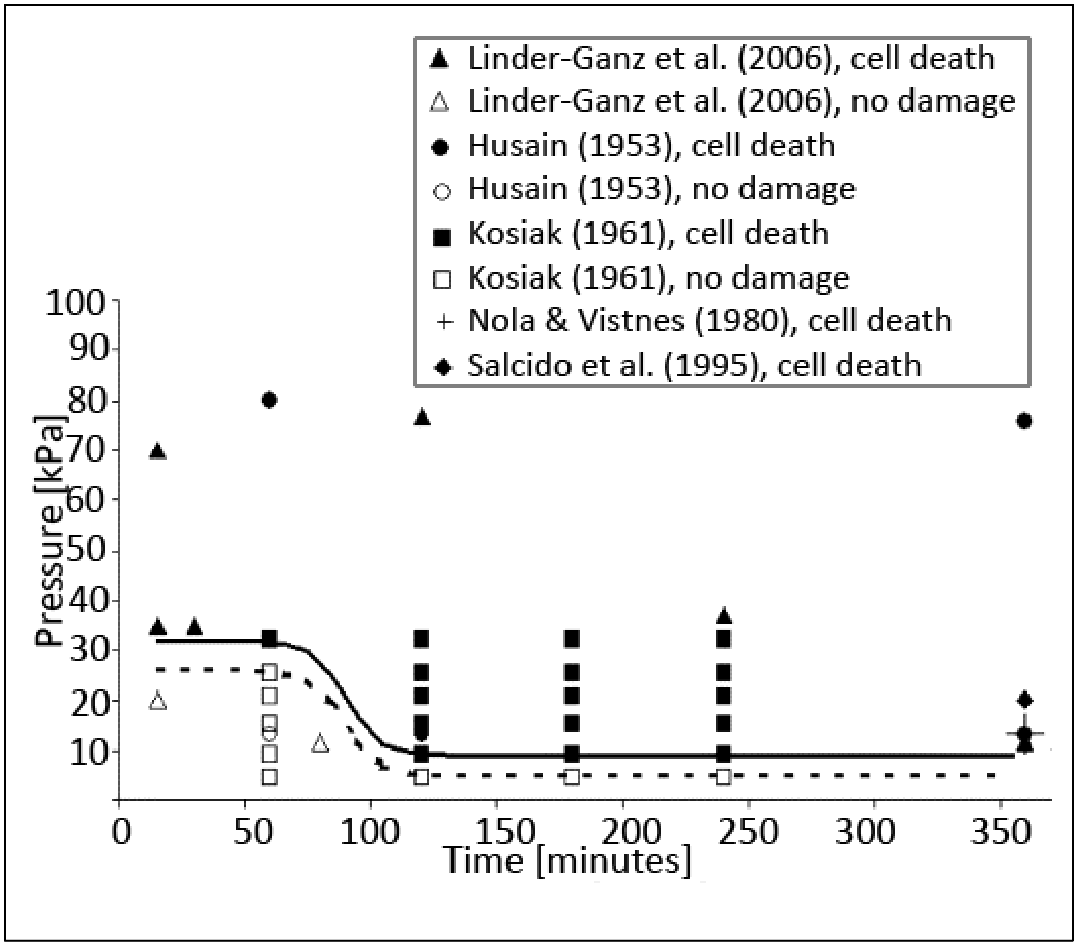

Figure 3-6: Pressure-time cell death threshold for muscle tissue of rats. This figure is from the study conducted by Linder Ganz et al. and compares the values obtained by various researchers. Reproduced from Linder Ganz et al., 2006.

The values of MH and MW, which were a measure of soft tissue thickness, were compared between the model and the MRI scans from the experiments. Though the percentage change of MW coincided with that of the model, the MH data for the model did not follow the trend seen in the experimental data. While the MH values found in experimental data decreased from normal to combined loading condition in the experiments, they stayed the same in the model. This could be because of the nature of the elastic isometric material properties assigned to the tissues, and is a limitation of the study. Future work will explore the application of visco-elastic material properties in order to investigate this difference.

The results of the study also indicated that muscle and skin tissues reacted differently to applied loads in terms of deformation and internal stresses. Muscle tissues displaced more than skin tissues. This trend was similar to those reported by other researchers (Makhsous et al., 2007; Nola and Vistnes, 1980). The difference in such response variation to applied loads has been dedicated to the difference in composition, and structure (Nola and Vistnes, 1980).

The model presented here fills a gap in the literature. This model not only includes shear loading in evaluations of stresses and strains but also is conducted with an anatomically accurate model. This study, combined with the author's prior work on blood flow and skin perfusion, provides much needed insight into the direction of pressure ulcer propagation (superficial or deep initiation), explores the two theories of PU mechanism (deformation versus reduced blood flow) and confirms that shear forces play a crucial role in tissue deformation and stresses and are likely to be more detrimental to tissue damage than normal forces alone.

4. PRESSURE ULCER RESEARCH: A NOVEL APPROACH FOR MODELING ARTERIAL TO VENOUS BLOOD FLOW VIA PERMEABLE MEDIA

4.1 Introduction

4.1.1 Overview

External forces acting on the body during daily routine actions such as sitting on a chair or lying on a bed for long periods of time can cause a decrease in blood flow to the tissues and underlying regions (Bouten et al., 2003). The effects of this decreased blood flow are more pronounced in the elderly and spinal cord injured and may result in tissue necrosis, leading to deep penetrating wounds called pressure ulcers (Bansal et al., 2005; Kosiak, 1961; Russo et al., 2008; Sugarman, 1985; Whitney et al., 2006; Zhang and Roberts, 1993).

When a person is seated on a wheelchair or lying on an inclined bed, there are normal and shear forces acting on the body (Bush and Hubbard, 2007; Mimura et al., 2009; Reuler and Cooney, 1981). The effects of normal loads on blood flow have been studied and reported by many researchers (Bansal et al., 2005; Bouten et al., 2003; Kosiak et al., 1958). However, few have researched the effects of combined loads (normal and shear forces) on blood flow in the deep vessels, and on superficial skin perfusion (Bennett et al., 1979; Manorama et al., 2013, 2010; Zhang and Roberts, 1993).

Previous work of the authors applied normal and combined loads (normal and shear loads) on the human forearm, and concluded that combined loads caused a greater decrease in superficial skin perfusion than normal loads alone. When the applied normal loads were doubled and no shear loads were applied, the decrease in perfusion was not significant, thus indicating that a combination of normal and shear loads is more detrimental than normal loads alone, with regard to skin perfusion (Manorama et al., 2010). Another study by the authors focused on the effects of normal and combined loads on deep vessel blood flow in the forearm artery and vein and achieved similar results, thus indicating that externally applied shear loads not only decreased the superficial skin perfusion but also the flow in the arteries and veins (Manorama et al., 2013).

There are two theories regarding the direction of ulcer propagation. One theory states that ulcers start at the skin level, and proceed inwards (Shea, 1975). The other theory states that an ulcer starts at the bone-muscle interface and proceeds outwards to the skin (Versluysen, 1986). In order to understand which mode of ulcer propagation is more likely to occur, a flow model is required that can compute the effective blood flow at various levels of the cross section of the body part (e.g. at the superficial level, and at the deep muscular level) under various external loads. Such a model could determine if the superficial or the deep tissue regions undergo a higher change in effective blood flow due to a given load, meaning a higher possibility for necrosis to take place in that region. However, in order to model this flow, simulation of the entire vascular system of the body segment would be necessary.

The vascular system is a complicated network of blood vessels, in which oxygenated blood from the heart is supplied to other parts of the body by deep arteries which branch into arterioles. The arterioles further branch out into tiny capillaries which supply oxygenated blood to the muscle, skin and other organs. Once the oxygen and other nutrients are absorbed, the deoxygenated blood is sent back from the capillaries through venules to the veins. Simulation of this entire network of blood vessels is complex. Instead, we proposed that modeling of blood flow from arteries to veins could be accomplished through a model with flow through porous media, where this complex system of vessels is replaced by a permeable medium. By assuming the muscle tissue to be permeable to blood from the arteries such that blood permeates radially outwards from the artery through the muscle to the vein, the arterial to venous blood flow can be modeled. When combined with a finite element (FE) model, the deformation due to applied loads could be related to effective blood flow at any region of cross section of the body part.

Thus, the objectives of this research were:

1. To devise an approach using permeable media to model the flow from artery to vein,

2. To input experimental values of arterial and venous blood flow rates into the model to determine an effective permeability value of muscle, and

3. To determine the change in effective permeability of muscle due to applied normal and combined loads, relating deformation to permeability and thus to effective blood flow of the body segment.

4.1.2 Permeability Models Approach

Permeability models have been employed by various researchers in the fields of geology, groundwater flow, reservoir engineering, and biomedical engineering (Baish et al., 1997; Butler et al., 1997; El-Shahed, 2003; Grobelnik et al., 2008; Huyghe et al., 1992; Nakayama and Kuwahara, 2008; Prosi et al., 2005; Vankan et al., 1997, 1996). Some studies have focused on the transport of proteins from the arterial lumen to the walls and inside the arterial walls (Karner et al., 2000; Stangeby and Ethier, 2002; Zunino, 2002), and other studies have used permeability concepts to study the dynamics of oxygen transport (Back et al., 1977; Ehrlich and Friedman, 1977; Rappitsch et al., 1997). A few researchers modeled blood perfusion using porous media but their methods and purpose were different from those of this study

(Huyghe et al., 1992; Vankan et al., 1997, 1996). Specifically, Huyghe et al. modeled the ventricle of a beating heart, assuming the myocardial tissue as a porous spongy material (Huyghe et al., 1992). Vankan et al. developed a poro-elastic model of rat muscle by assuming it to be a porous solid (Vankan et al., 1997, 1996). However, a study modeling the arterial to venous flow by assuming flow in smaller vessels to be permeable through the muscles, to understand the effects of external loads on blood flow has not been done before.

The approach taken to perform this flow analysis is inspired by models pertaining to groundwater flow. Concepts from groundwater flow using porous media are discussed in this section and then are applied to our human forearm model.

Groundwater flow analysis is predominately based on Darcy's law. Darcy's law in its broadest form relates the volumetric flow rate to the pressure gradient (Darcy, 1856; Hall and Hoff, 2009). It is the pressure gradient that drives the permeable flow. Consider a circular well at the center of a circular aquifer of height, H (Figure 4-1). The differential form of radial flow equation of Darcy's law is used to compute the flow rate from the aquifer to the well using the relation:

$$Q = \frac{-KA}{\mu}\frac{dP}{dR}$$

where Q is the volumetric flow rate from the aquifer to the well, and also the flow rate through the well since Q is conserved; μ is the viscosity of the fluid; A is the area normal to permeable flow; R is the radial distance along the groundwater flow path; $\frac{dP}{dR}$ is the pressure gradient between the well and reservoir; and K is the permeability of the soil. The unit of permeability is Darcy, where 1 Darcy equals 10^{-12} m^2.

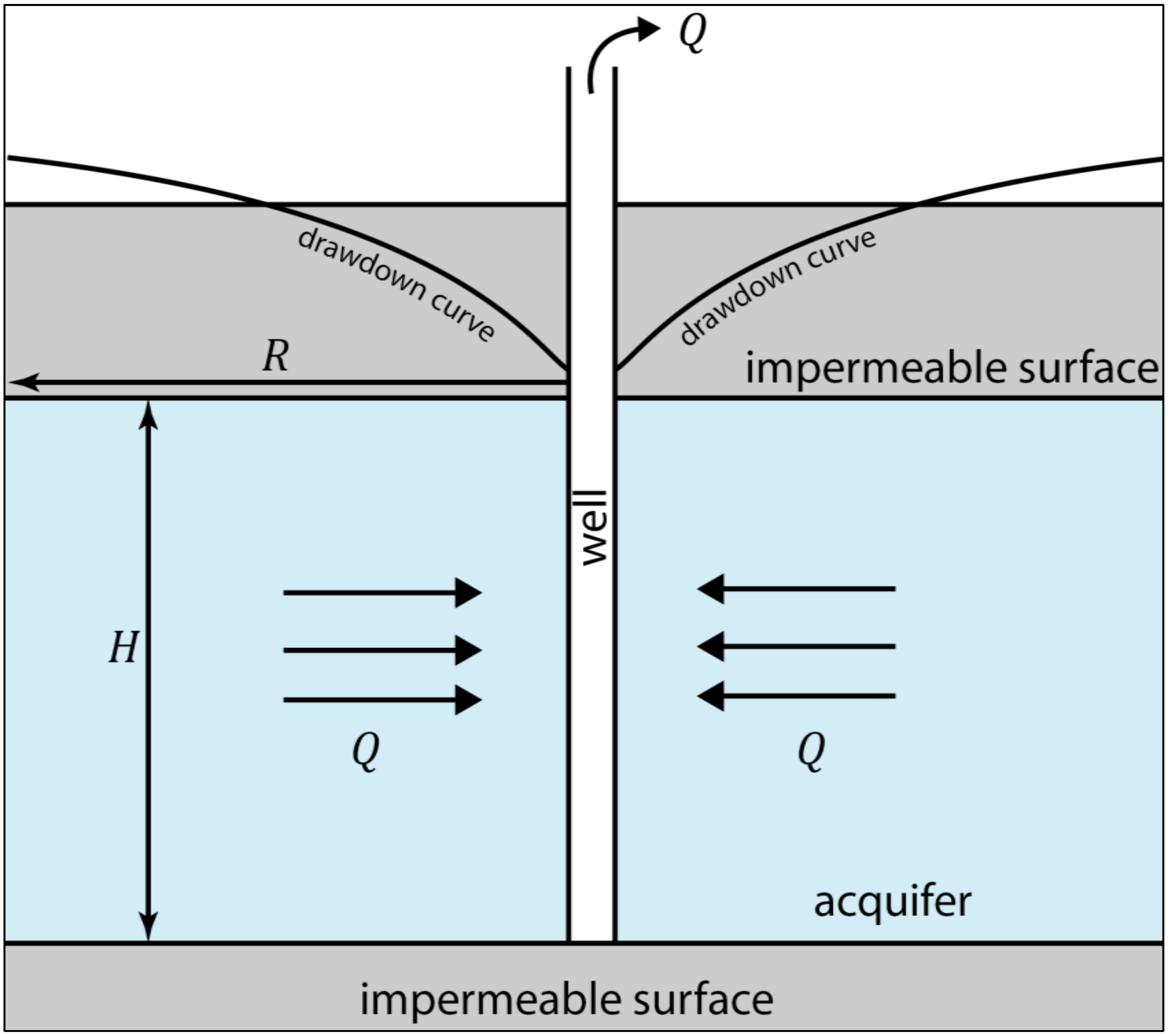

Figure 4-1: Steady flow to a completely penetrating well in a confined aquifer. Dotted regions represent the permeable aquifer surface, and checked regions represent the impermeable surface. The drawdown curve shows the variation of pressure drawdown with distance.

For a cylindrical aquifer, $A = 2\pi RH$, where H is the height of the aquifer, and the equation takes the form:

$$Q = \frac{-2\pi KHR}{\mu}\frac{dP}{dR}$$

For steady flow, the flow rate of water flowing through the well is also the flow rate through any cylindrical shell around the well. Separating the variables and integrating between two values of radial distances given by R_1 and R_2 gives the Thiem equation, where P_1 and P_2 are pressures at R_1 and R_2 respectively, and P_2-P_1 is called the pressure drawdown (Elango and Sivakumar, 2005; Verruijt, 1970).

$$P_2 = P_1 - \frac{\mu Q}{2\pi KH} \ln\left(\frac{R_2}{R_1}\right)$$

Thus, by imagining the vein of forearm to be a well, and the muscle tissue as an aquifer, the permeating flow from the muscle tissue to the vein can be described using the Thiem equation. However, the forearm model has an artery in addition to the vein, which supplies blood into the muscle which then permeates into the vein. In order to describe this flow, the principle of superposition in groundwater flow concepts needs to be applied. According to the principle of superposition in groundwater flow, if there are two or more wells, the total drawdown is equal to the sum of drawdown of each individual well. This principle is used to determine well flow near a stream and to understand what fraction of the pumping is derived from the stream. In such a case, an imaginary recharge well is placed directly opposite and at the same distance from the stream as the real well (Figure 4-2). A recharge well is a well through which water is added to an aquifer. Hence, the resultant drawdown of the real well is given by the algebraic sum of the drawdown of the real well and the buildup of the recharge well (Verruijt, 1970).

For this work, we apply the concept of an aquifer with porous media and wells to the blood flow in the forearm model. In this model, the artery is comparable to the recharging well, the vein is comparable to the draining well, and the aquifer is comparable to the cross section of the forearm muscle (Figure 4-4). These principles can be employed to model the blood flow from the artery through the muscle to the vein. However, since the cross section of the forearm is complicated and has obstructions such as the bones which are impermeable to blood flow, fluid flow simulation software will be required to solve the problem. An analytical solution, though, can be computed for a simplified 2D cross section, which can be used as starting point for the models, to reduce the number of iterations.

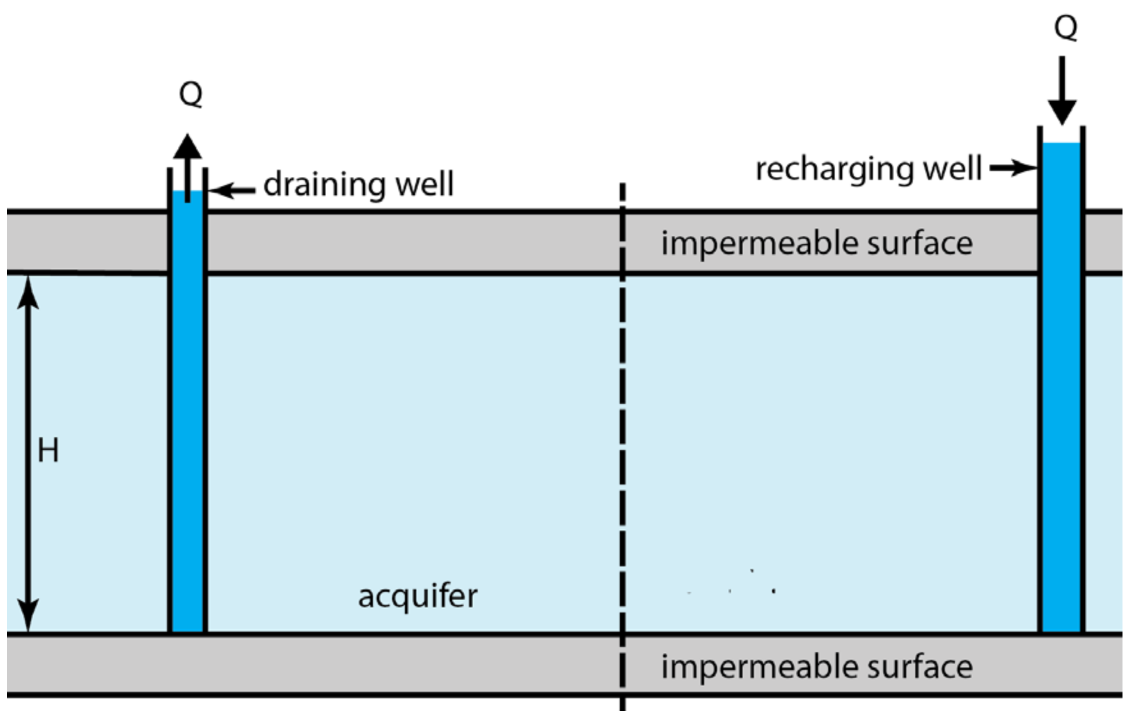

Figure 4-2: A system depicting a recharging well and drawing well in a confined aquifer. Dotted regions represent the permeable aquifer surface, and checked regions represent the impermeable surface. Fluid from recharging well permeates through the aquifer and flows into the draining well. This approach is used to model blood flow permeating from the artery through the muscle to the vein.

The governing equations for this flow are the Navier-Stokes equations for incompressible flow, which are presented below in cylindrical coordinates:

Continuity equation:

$$\frac{1}{r}\frac{\partial(ru_r)}{\partial r} + \frac{1}{r}\frac{\partial(u_\theta)}{\partial \theta} + \frac{\partial u_z}{\partial z} = 0$$

Momentum equations:

$$\rho\left[\frac{\partial u_r}{\partial t} + u_r\frac{\partial u_r}{\partial r} + \frac{u_\theta}{r}\frac{\partial u_r}{\partial \theta} - \frac{{u_\theta}^2}{r} + u_z\frac{\partial u_r}{\partial z}\right]$$

$$= -\frac{\partial P}{\partial r} + \rho g_r$$

$$+ \mu\left[\frac{1}{r}\frac{\partial}{\partial r}\left(r\frac{\partial u_r}{\partial r}\right) - \frac{u_r}{r^2} + \frac{1}{r^2}\frac{\partial^2 u_r}{\partial \theta^2} - \frac{2}{r^2}\frac{\partial u_\theta}{\partial \theta} + \frac{\partial^2 u_r}{\partial z^2}\right]$$

$$+ S_{DR}$$

$$\rho\left[\frac{\partial u_\theta}{\partial t} + u_r\frac{\partial u_\theta}{\partial r} + \frac{u_\theta}{r}\frac{\partial u_\theta}{\partial \theta} + \frac{u_r u_\theta}{r} + u_z\frac{\partial u_\theta}{\partial z}\right]$$

$$= -\frac{1}{r}\frac{\partial P}{\partial \theta} + \rho g_\theta$$

$$+ \mu\left[\frac{1}{r}\frac{\partial}{\partial r}\left(r\frac{\partial u_\theta}{\partial r}\right) - \frac{u_\theta}{r^2} + \frac{1}{r^2}\frac{\partial^2 u_\theta}{\partial \theta^2} - \frac{2}{r^2}\frac{\partial u_r}{\partial \theta} + \frac{\partial^2 u_\theta}{\partial z^2}\right]$$

$$+ S_{DR}$$

$$\rho\left[\frac{\partial u_z}{\partial t} + u_r\frac{\partial u_z}{\partial r} + \frac{u_\theta}{r}\frac{\partial u_z}{\partial \theta} + u_z\frac{\partial u_z}{\partial z}\right]$$
$$= -\frac{\partial P}{\partial z} + \rho g_z + \mu\left[\frac{1}{r}\frac{\partial}{\partial r}\left(r\frac{\partial u_z}{\partial r}\right) + \frac{1}{r^2}\frac{\partial^2 u_z}{\partial \theta^2} + \frac{\partial^2 u_z}{\partial z^2}\right]$$
$$+ S_{DR}$$

where ρ is density; P is pressure; g is gravitational acceleration vector; u_r, u_θ, u_z are velocity vectors; μ is viscosity; and S_{DR} is the sink term added to the momentum equations to account for the additional pressure loss due to porous media (Alam et al., 2011; Hunt and Tien, 1988). In regions of axial flow through the vessels, S_{DR} takes zero value, whereas in regions representing the porous flow, it takes the following forms, defined by Darcy's law:

$S_{DR} = -\frac{\partial P}{\partial r} = \frac{\mu}{K}u_r$ in radial direction;

$S_{DR} = -\frac{1}{r}\frac{\partial P}{\partial \theta} = \frac{\mu}{K}u_\theta$ in tangential direction;

$S_{DR} = 0$ in axial direction;

where K is permeability.

Several inputs were provided for the model. Details regarding these inputs are described in the model construction sub-section of the methods section. However, in general, the values of volumetric flow rate were the inputs based on experimental data. Also, pressure, density and viscosity were prescribed, based on data sets provided in the literature. From the volumetric flow rate and the cross sectional area of the vessels, the internal velocities u_r, u_θ, and u_z values were calculated by the software. In terms of permeability, an initial guess was necessary for the iteration process. This initial guess was based on numerical calculations of a simplified model.

4.2 Methods

4.2.1 Overview

The method presented here is of a novel approach to model the arterial to venous flow by assuming that the muscles are permeable to blood flow. In the current study, the flow from the anterior interosseous artery (AIOA) to the basilic vein (BV) of the forearm is modeled. Figure 4-3 shows a Magnetic Resonance Image (MRI) cross-sectional slice of the forearm, identifying the AIOA and BV. The blood flow velocities in these vessels, as well as the 3D geometry of the forearm were obtained from the experiments conducted in a MRI setting (Chapter 2), while the deformation due to normal and combined loads were obtained from FE simulations conducted on the 3D model of the forearm (Chapter 3).

4.2.2 Participant

The model is individual- specific, and based on a healthy young male (age: 25 years), with a mass of 68 kg and height of 178 cm. The participant had no prior vascular issues. The MRI experiment was conducted after obtaining written consent, and the research methods were approved by the Michigan State University Institutional Review Board.

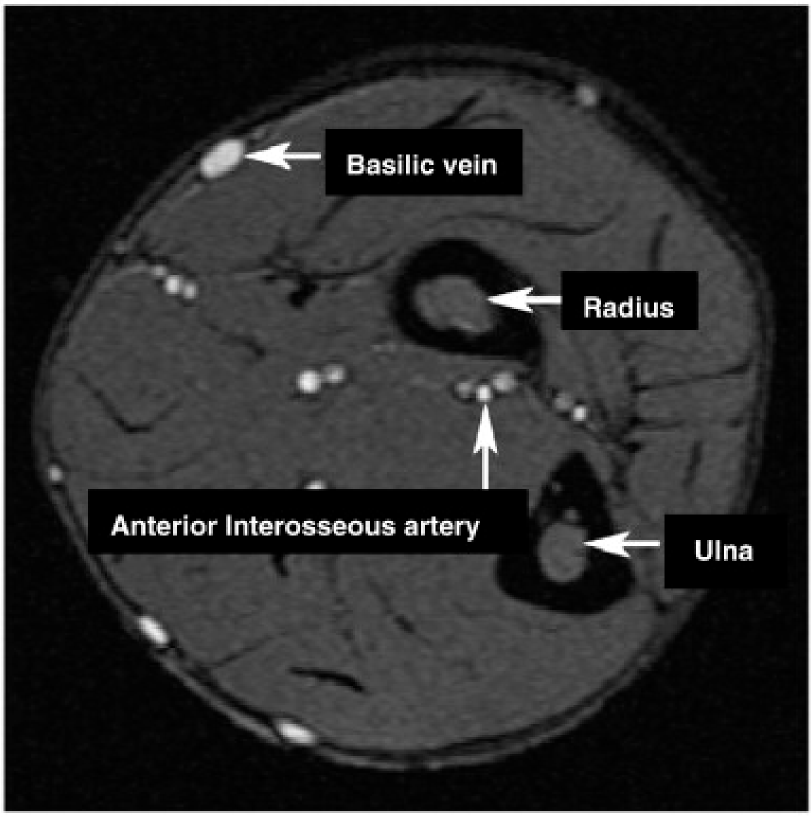

Figure 4-3: MRI cross-sectional slice showing the anterior interosseous artery and basilic vein, along with the bones, muscle, and skin of the forearm

4.2.3 Experiment

The blood velocity and cross sectional areas necessary to obtain blood flow rate (Q) were obtained from data collected on the participant in an MRI scanner. The participant was asked to lay prone inside the MRI scanner, with his right arm extended in front of him. To obtain the anatomical geometry of the forearm, showing the bones, muscle, skin, and larger blood vessels, a Time-of-Flight (TOF) scan was conducted while in the MRI. The TOF scan delivered 52 cross-sectional image slices of the forearm section, with an inter-slice thickness of 0.2 cm.

Next, an angiography scan using Phase-Contrast Imaging was conducted to measure the baseline blood flow in the AIOA and BV of the forearm. Following this, a normal load of 20 mm Hg over an area of 82 cm^2 was applied on the forearm, and the blood flow was recorded again. Finally, a shear load of 15.6 N was applied in addition to the normal load specified above, and the blood flow values were recorded. A detailed description of the methodology and results of the experiment can be found in Chapter 2 of the dissertation.

4.2.4 FE simulation

A 3D model was constructed and meshed using the TOF images from the experiments. The geometry pertaining to this model was the baseline "no load" geometry of the forearm. Two simulations were conducted on the model—1) Normal load 2) Combined loads (normal plus shear load). The values of normal and shear forces applied in the simulations were same as those applied in the experiments. Results of these simulations provided two deformed geometries corresponding to the two sets of loads. A total of three geometries of the forearm were developed, corresponding to baseline, normal, and combined loads. These three models served as inputs for constructing the permeability models.

Detailed methodology and results of these simulations can be found in Chapter 3 of this dissertation.

4.2.5 Analytical solution of permeability

The methodology involved an iterative process to determine the permeability of the muscle and therefore a starting value of permeability was required for the first iteration.

In terms of permeability values, a wide range of possibilities exists for the array of permeable materials. For example, the permeability values of different materials in geology vary from the order of 10^{5} Darcy to 10^{-8} Darcy (Bear, 2013; Hall and Hoff, 2009). In biological models, the permeability of a blood clot has been calculated to be 100 Darcy (Carr et al., 1977), and that of a human aortic wall has been determined to be 2×10^{-6} Darcy (Stangeby and Ethier, 2002). Hence, for this study it was important to start with a value that would be close to the actual value, so that the number of iterations and thus run-time could be minimized. To obtain this initial value, an analytical value of permeability was calculated for a 2D side-section of the baseline model.

The baseline model was cut using a cutting plane that passed through the cross section along the length of the AIOA and BV (Figure 4-4). Calculations for analytical permeability were made for the cut surface, by simplifying the geometries and neglecting the obstructions between the two vessels. Specifically, as seen in Figure 4-4, the cut surface has bones obstructing the area between the two vessels. Also, the artery and vein were not of uniform cross sectional area and were not straight cylinders. Hence, for the analytical calculations, the bones were neglected and the vessels were assumed to be straight cylindrical sections.

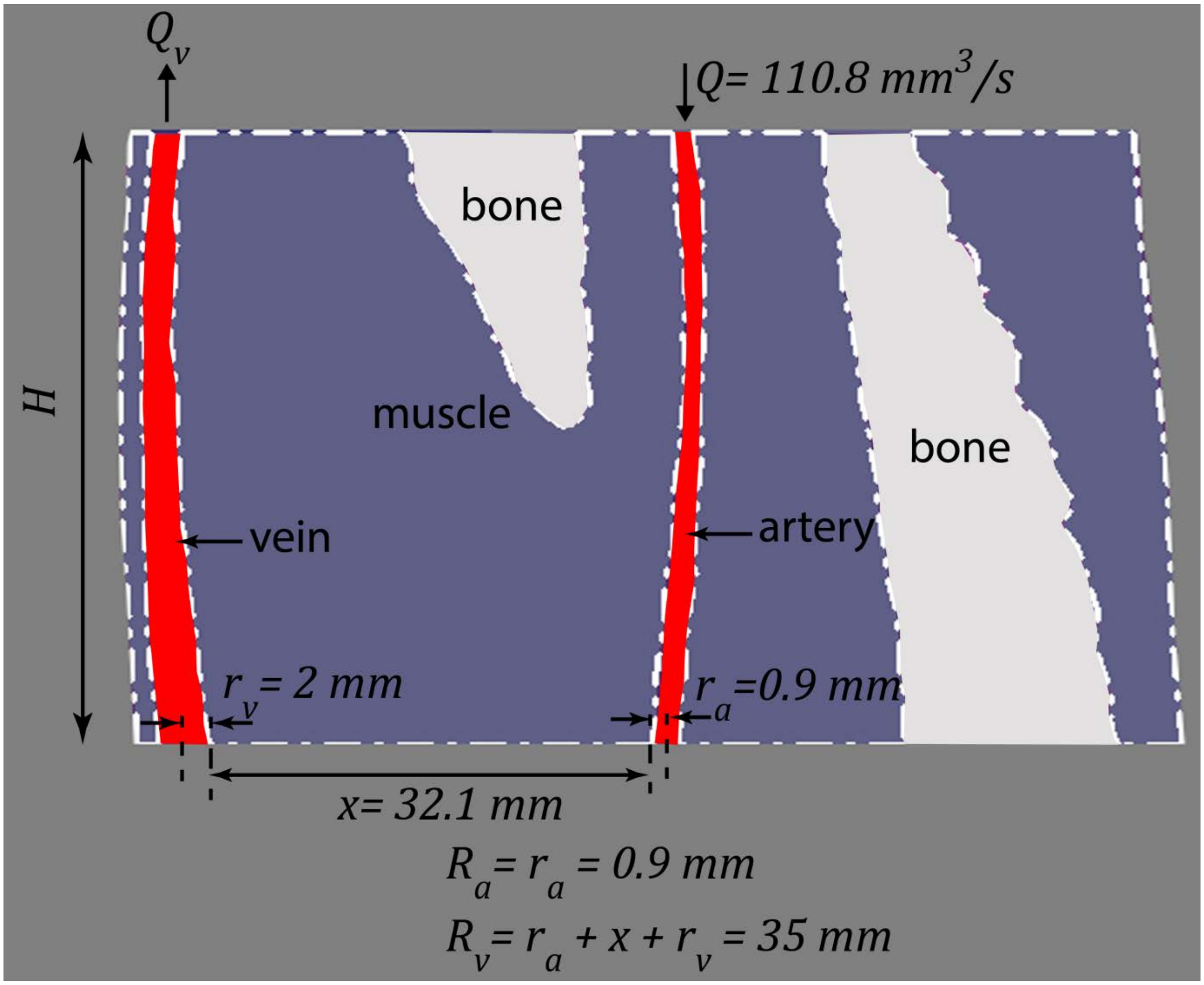

Figure 4-4: Side section of the forearm model with the artery, vein, and muscle representing a recharging well, draining well and aquifer respectively. r_a represents arterial radius, r_v represents venous radius, R_v represents the distance from center of artery to center of vein.

The muscle tissue was modeled as an aquifer with the artery serving as a recharge well, and the vein a draining well. Further, a constant flow rate of 110.8 mm^3/s (the experimental flow rate in AIOA for baseline condition) was assumed for the artery.

Following the principles of superposition of pressure drawdowns, the total pressure gradient between the artery and vein was given by:

$$\Delta P = \frac{\mu Q}{2\pi K H} \ln \frac{R_a}{R_v}$$

where R_a is the distance from the center of the artery to its periphery, R_v is the distance from center of the artery to center of the vein. The permeability value obtained from the calculations was used as a starting value for the first iteration of the permeability model, and is presented in the Results section of this chapter.

4.2.6 Model construction

(i) Geometry

Three geometries of the forearm, corresponding to baseline, normal, and combined load conditions were obtained from FE simulations. In order to reduce computational times during flow simulations, a 2 mm thick slice of each model corresponding to the proximal end of the forearm was split from the original geometries to be used for the permeability models (Figure 4-5). The baseline model was imported into Autodesk Simulation CFD (Autodesk Inc., San Rafael, CA, USA), in order to carry out simulations.

(ii) Material properties

The materials present in this model were blood and muscle. Blood was modeled as an incompressible Newtonian fluid in the axial flow regions in the artery and vein, and allowed for non-Newtonian flow in the permeable regions. Although the blood flow in the larger vessels such as arteries is known to be Newtonian, the blood flow in capillaries is commonly modeled as non-Newtonian owing to the rise in viscosity leading to Fahreaus-Lindquist effect (Fournier, 2011; Ku, 1997). The material properties included a density of 1.003 g/cm^3 assigned from the software material library (Autodesk, 2013), and was a little lower than blood density range (1.02-1.11 g/cm^3) reported by other researchers (Cebral et al., 2002; Fournier, 2011; Kenner, 1989).

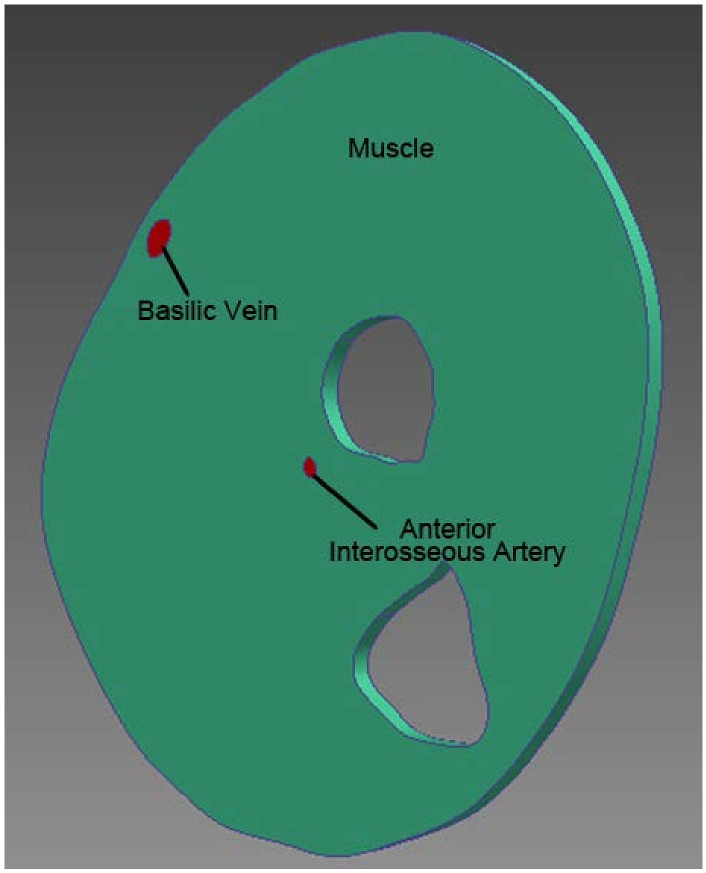

Figure 4-5: Permeability model of the forearm pertaining to baseline condition, showing the muscle, vein, and artery

The viscosity was governed by power law. The cutoff viscosity, which was the viscosity of the fluid as a Newtonian fluid, was assigned to be 0.12 Pa-s (Pascal second). The viscosity coefficient, which was the viscosity at which the fluid became non-Newtonian, was set at 0.036 Pa-s. The strain rate at which the fluid became non-Newtonian, also known as the cutoff strain rate, was assigned a value of 0.065. The power law exponent was set at -0.397, with a value of 0 representing a Newtonian fluid, and positive and negative values representing shear thickening and shear thinning fluids respectively. These values were assigned from the software material library (Autodesk, 2013). The assigned values were verified from trial simulations which, at the arterial and venous regions showed viscosity in the range of 3-4 centipoise, and were in accordance with values from previous literature (Cebral et al., 2002; Fournier, 2011; Ku, 1997).

The muscle tissue was modeled as a distributed resistance, which denotes a permeable material. The permeability values in the radial and tangential directions were assigned the value from the analytical calculations, whereas in the axial direction, permeability was set to zero. This constraint was included to be consistent with the assumptions of groundwater flow that the permeating radial flow through the aquifer is normal to the axial flow in the well.

(iii) Boundary conditions and analysis parameters

The pressures on the arterial and venous ends were set to 80 mm Hg and 8 mm Hg respectively. These values represented standard arterial and venous pressures in these vessels, as determined by previous researchers (Coccagna et al., 1971; Ochsner et al., 1951; Pollack and Wood, 1949). The permeable flow was driven by this pressure gradient between the artery and vein.

Since arterial and venous flow are in opposite directions, the arterial inlet and the venous outlet were on the same surface i.e. proximal end of the model. The volumetric flow rate in the arterial inlet was assigned to 110.8 mm^3/s, which was obtained from the MRI experiments. In order to conserve the flow rate, the flow in the distal end was blocked by assigning zero axial flow to the arterial outlet and venous inlet (Figure 4-6). Also, in the muscle region, the flow in the axial direction was set to zero, in order to keep the flow streamlined, and be consistent with assumptions of groundwater flow modeling.

The flow in the model was assigned to be a steady state laminar incompressible flow. The model was meshed with a total of 9286 elements. The modified Petrov-Galerkin advection scheme was chosen for the simulations, since it is specific to pressure-driven flow, and produces conservative results (Autodesk, 2013).

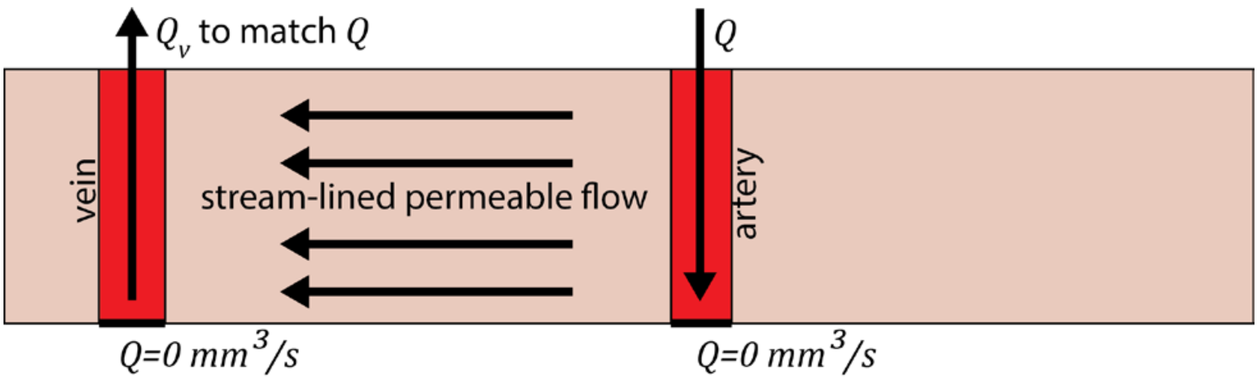

Figure 4-6: Conceptual diagram showing side section of the model, with the flow rate boundary conditions at the arterial inlet and outlet, and the venous inlet. *Q* denotes the experimental value of arterial blood flow. The flow in the permeable muscle region is limited to the radial and tangential directions to make it stream-lined. The permeability value of muscle is chosen so the flow rate at the vein outlet matches the flow at the arterial inlet.

(iv) Iterative process

The model was simulated in Autodesk Simulation CFD in multiple iterations, and after solving for each iteration, the muscle permeability (K) and venous flow rate (Q_V) values were plotted. For each iteration, the value of K was modified from the previous iteration and the value was plotted. The aim was to change the K values in each iteration until Q_V matched the flow rate in the artery.

A minimum of six iterations were performed by varying the K values in each iteration and plotting the K and Q_V values. Following this, the plot points were curve-fit to a second-order polynomial equation with Q_V and K as the variables. The, the equation was solved for Q_V, where Q_V equaled the arterial flow input (Q), and the corresponding K was obtained.

This process was repeated for each of the three models (baseline, normal, combined loading). By using the corresponding flow rates as inputs and the iterative process, the permeability values were obtained for each of the three models.

4.3 Results

Analytical calculation of permeability from the 2D side cross section of the baseline model yielded a permeability value of 401.6 Darcy. This value of permeability was used as a starting value for the baseline model. Figure 4-7 presents the results of this simulation, showing the flow lines from the AIOA to the BV on the baseline model.

A plot of Q_V vs. K for the baseline model is shown in Figure 4-8-a. When fit to a second order polynomial equation, the following equation was obtained.

$$Q_V = -(5 \times 10^{-5})\, K^2 - 0.2126\, K + 47.137$$

This equation, when solved for K using a Q_V value of 110.8 mm^3/s obtained from the MRI experiments, yielded the permeability value of the baseline model to be 645.2 Darcy.

For the normal load condition, a plot of Q_V vs. K is shown in Figure 4-8-b. When fit to a second order polynomial equation, the following equation was obtained.

Q_V = - (3 x 10^{-4}) K^2 + 0.1111 K - 47.696

When solved for K using a Q_V value of 83.2 mm^3/s, a permeability value of 576.0 Darcy was obtained.

For the combined loading condition, a plot of Q_V vs. K is shown in Figure 4-8-c. When fit to a second order polynomial equation, the following equation was obtained.

Q_V = (1 x 10^{-4}) K^2 – 0.3095 K + 52.273

When solved for K using a Q_V of 50.3 mm^3/s, the permeability value of 377.3 Darcy was obtained.

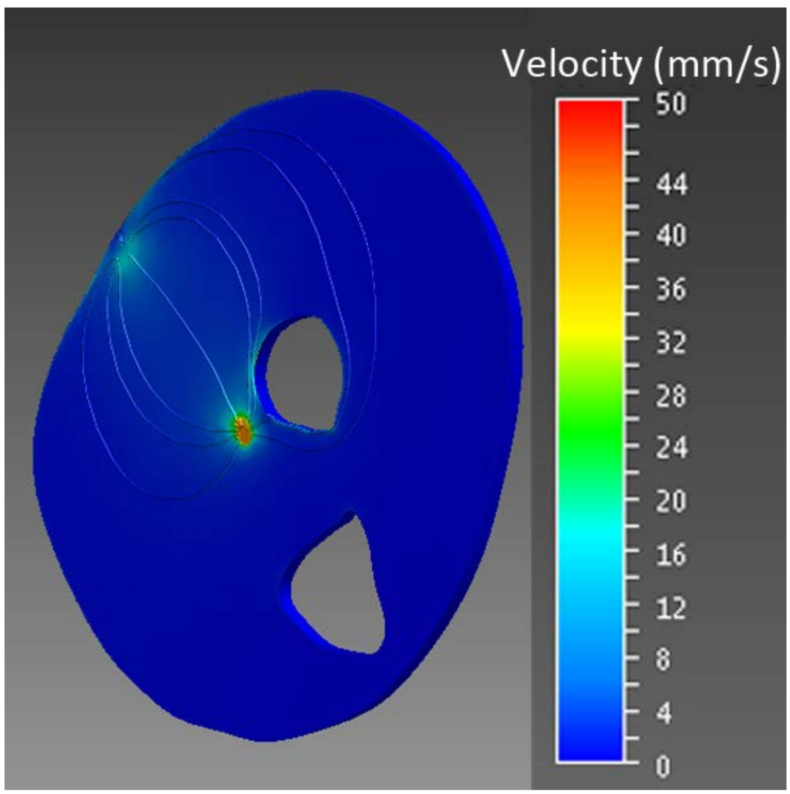

Figure 4-7: Results of the Baseline (no load) model, showing blood flow permeating from the artery through the muscle into the vein

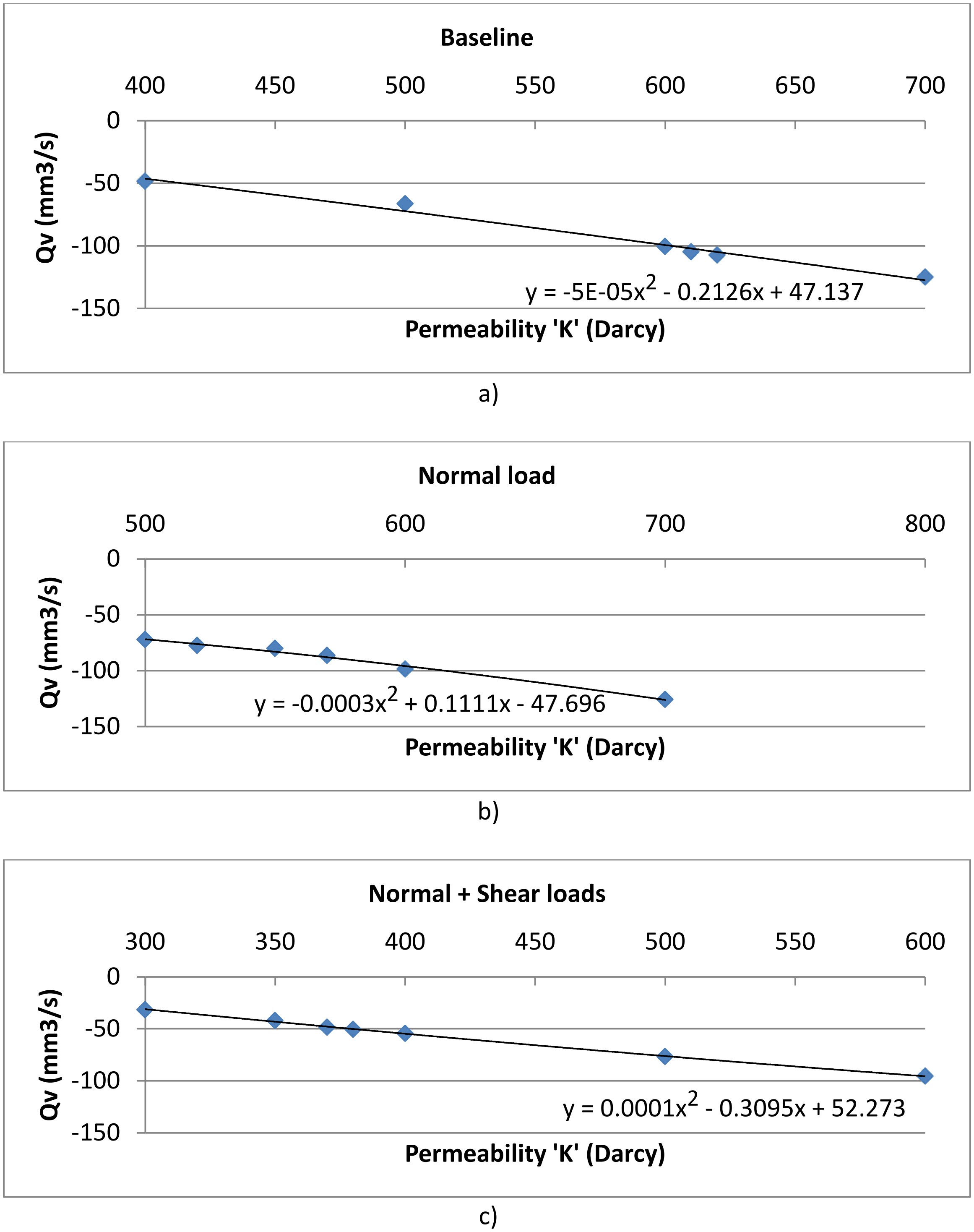

Figure 4-8: Plots of volumetric flow rate (Q_V) in the basilic vein vs. muscle permeability, best fit to a second order polynomial equation, in a) Baseline condition b) Normal load condition c) Combined (normal plus shear) load condition

4.4 Discussion and Conclusions

The approach presented in this chapter, which models the movement of blood from an artery to a vein by assuming muscle tissues as porous media, is a novel method to model the complex network of arterioles, venules and capillaries.

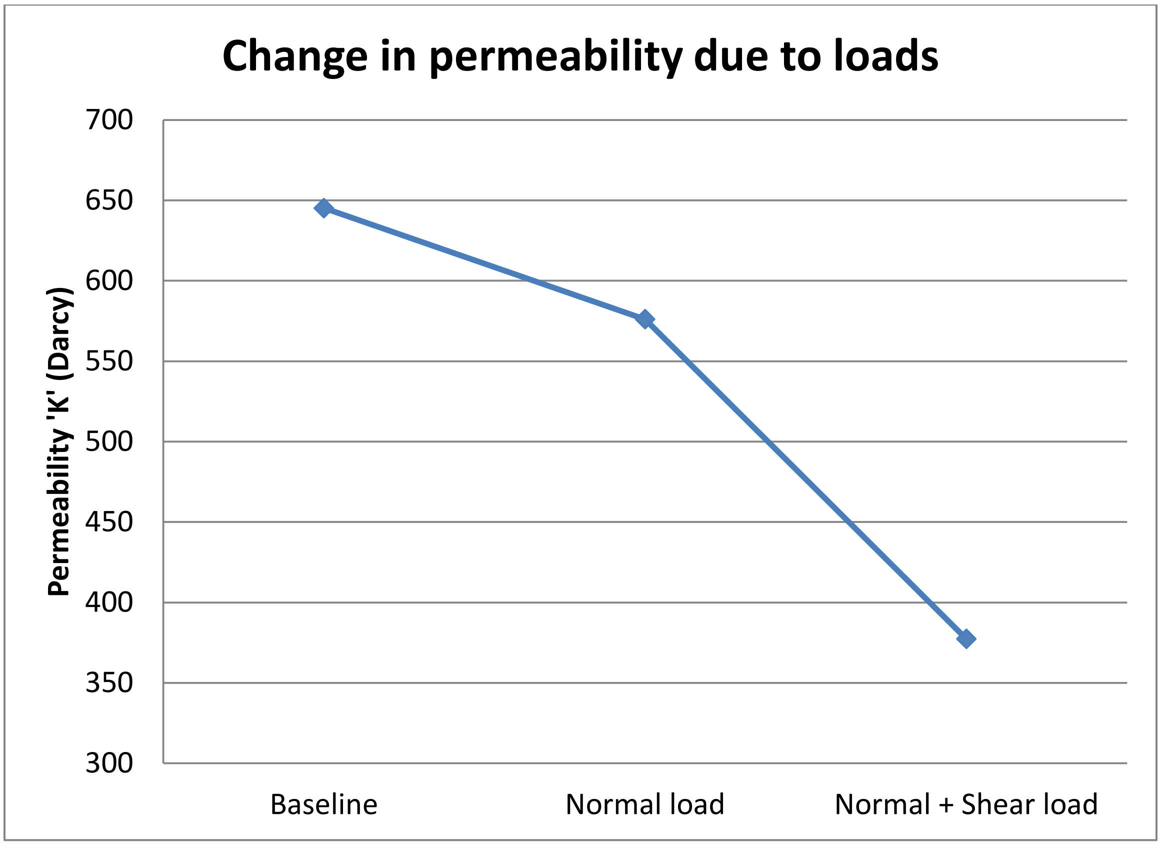

Figure 4-9: Change in muscle permeability in relation to externally applied normal loads and combined loads of normal and shear

The approach was developed based on the theory of groundwater flow and then adapted to the forearm. After development of the approach, it was performed on an individual-specific model of the forearm. In this application, changes in muscle permeability due to externally applied loads were evaluated. Three values of muscle permeability were determined which corresponded to baseline, normal load, and combined loads applied to the skin. These permeability values fell within the range of permeability of various permeable biological materials (10^5 Darcy to 10^{-8} Darcy) described in previous literature (Bear, 2013; Carr et al., 1977; Hall and Hoff, 2009; Stangeby and Ethier, 2002). The results of this model demonstrated that if the muscle is assumed as a permeable medium, the permeability decreases with the application of normal load, and decreases further with the addition of shear load to the normal load (Figure 4-9).

The method presented here is novel and is advantageous over the conventional modeling approaches. Although the concepts of porous media have been used in groundwater flow, petroleum reservoir engineering, and even in areas of biomedical engineering, a model representing the arterial to venous blood flow in a body segment by a permeable flow to study the relation between deformation and blood flow has not been developed.

This method has strong applications for pressure ulcer research. Of specific interest are the effects that forces applied on the skin have on blood flow. This relationship is important because the forces acting on the body segment decrease the blood flow thus increasing the potential for tissue necrosis and pressure ulcers. Using this approach the effective blood flow rate at any region in the model could be determined by selecting a Region of Interest (ROI). Thus, for instance, two ROI's could be selected— one at the superficial level and one at the deep level of the model. If the changes in effective blood flow at each of these regions during the three conditions are compared, it will be possible to understand if it is the superficial skin regions or the deep muscle regions that undergo a greater decrease in blood flow due to different loading scenarios. This will help improve the understanding of where ulcers are likely to initiate.

The current model, however, has limitations. First, the volumetric flow rate is assumed to be conserved, which makes the venous flow rate the same as the arterial flow rate. This is not the case in reality where each artery and vein has different flow rates owing to the differences in velocities, and cross sectional areas. Also, this model consists of a single artery and single vein, which renders all the flow lines from the artery to the vein, making regions far from these two vessels low in blood flow. In reality, the forearm has four major arteries, and at least eight veins. Future work will include all the arteries and veins in the forearm, which will give a more accurate representation of muscle permeability. Also, by including all arteries and veins, conservation of flow rate is applied to the entire system, in which case the veins will not have the same flow rate as the arteries, since they are larger in number than the arteries. Future work will aim at better anatomical representation and improving the accuracy of the value of permeability by inputting the flow rates of all the arteries and veins from experiments into the model. Another limitation to this work is that the sensitivity of changing the material property values such as density and viscosity was not studied. Future work will also include the study of how varying other parameters affect permeability.

Being able to determine the relation between external forces and the internal vascular flow is important in pressure ulcer research, since external forces cause a decrease in blood flow and thus, a decrease in transport of oxygen and other nutrients to the tissues. This causes tissue necrosis, leading to pressure ulcers. Understanding this relation will help in developing better ulcer prevention methods and in improving seating designs. In addition, these results will provide a value of effective permeability of muscle which will be useful in further studies that employ similar modeling approaches.

In conclusion, the approach presented in this paper is a seminal study to model the vascular network using permeability theory and is a beginning step for further research in this area. The results of the current model strengthen the fact that shear forces are more detrimental than just normal forces in leading to pressure ulcers, and thus should be given more consideration in ulcer prevention measures.

5. EVALUATION OF THE RELATIONS OF SOFT TISSUE THICKNESS AND LOCAL SKIN TEMPERATURE WITH FOREARM BLOOD FLOW AT VARIOUS LOADS

5.1 Introduction

5.1.1 Overview

The National Pressure Ulcer Advisory Panel (NPUAP) and the European Pressure Ulcer Advisory Panel (EPUAP) define a pressure ulcer (PU) as a “localized injury to the skin and/or underlying tissue, usually over a bony prominence, as a result of pressure, or pressure in combination with shear force” (EPUAP, 2009; NPUAP, 2009).

PUs are a major health concern throughout the world, and are most common in the elderly and those with limited mobility. The estimated prevalence of PUs in the United States is 1.3 to 3 million (Lyder, 2003) while the United Kingdom reports 412,000 incidences annually (Bennett et al., 2004). The PU prevalence in healthcare settings was estimated at 26% in Canada, and 23% in German hospitals and nursing homes (Lahmann et al., 2005; Vanderwee et al., 2007; Woodbury and Houghton, 2004). Among people under medical care, the reported PU incidence rates as high as 38% for hospital-admits, 24% for long term care, and 17% for home care patients (Cuddigan et al., 2001). A new PU can increase the duration of a patient’s hospital stay by five times (Lazarus et al., 1994). Recurrence rates for PUs are as high as 39% (Keys et al., 2010). Furthermore, PUs are correlated with two times the likelihood of mortality (Brem and Lyder, 2004).

PUs are a financial burden to the healthcare system. The cost of treatment of a PU can be as high as $40000 per ulcer (Bergstrom et al., 1992). In the United Kingdom, the average hospital cost of treating PUs has been estimated to be £600,000–£3 million per year (Nhs.uk, 2009). Approximately 75% of PU-diagnosed patients are 65 years and older (Russo et al., 2008), and 50% of these older individuals are bedridden or wheelchair-bound (Bansal et al., 2005; Sugarman, 1987).

5.1.2 Mechanism and factors

PUs develop in regions of the body that are exposed to pressure between bony regions and an external surface. This pressure caused by normal forces (i.e. forces acting perpendicular to the skin) leads to a decrease in blood flow resulting in obstruction of transport of oxygen and nutrients to the tissues, leading to tissue necrosis and eventually to PUs (Bouten et al., 2003).

Pressure is not the only factor leading to PUs, since an individual lying on an inclined bed, or seated in a chair, is subjected to not only normal forces but also shear forces (i.e. forces acting tangential to the skin) between the body and support surface. A previous study by the authors evaluated the effects of normal loads and self-applied shear loads on skin perfusion (i.e. blood flow in the superficial skin capillaries) in the forearm of seated individuals. The results indicated that perfusion decreased more so due to combined normal and shear loads than due to just normal loads, thus suggesting that combined loads were more detrimental than normal loads in leading to tissue necrosis.

Other factors thought to play a role in tissue damage leading to PUs are Body Mass Index (BMI) and local skin temperature (Kottner et al., 2011; VanGilder et al., 2009).

5.1.3 Soft tissue thickness

Researchers have stated that slender people with low BMI might be at a higher risk of developing PUs (Kottner et al., 2011; VanGilder et al., 2009). It has also been suggested that soft tissue thickness measurement could serve as a predictor of PU risk (Clark et al. 1989). However, data relating soft tissue thickness to blood flow at various loads are not available.

Such information is necessary to understand if shear force is more detrimental to blood flow for individuals with lower soft tissue thickness values. If so, the individuals with lower soft tissue thicknesses are likely to be at an increased risk for tissue damage.

5.1.4 Local skin temperature

In the context of PUs, microclimate refers to skin temperature and moisture at the skin-support surface interface (Clark et al., 2010). Increasing skin temperature increases perspiration, thereby increasing the moisture and thus affecting microclimate (Lachenbruch, 2005), and raised microclimate is a recognized risk factor leading to PUs (Bergstrom and Braden, 1992; Nixon et al., 2000). A few studies have explored the effects of local skin temperature, in relation to PUs (Brienza and Geyer, 2005; Kokate et al., 1995). However, a study evaluating the effects of combination of temperature and load variation on blood flow has not been conducted, and is important. For instance, when shear load and microclimate are evaluated separately they may not appear to be problematic, but the combined effects of these two factors may put the individual at a higher risk for developing a PU. Hence, a study focusing on the combined effects of these two factors is necessary and will increase the knowledge base with regard to how they interact in the context of tissue damage.

5.1.5 Objectives

The objectives of this study were:

1) To determine if a relationship exists between soft tissue thicknesses and blood flow with varied loading conditions.

2) To measure the effects of localized skin temperature on blood flow changes with varied loading conditions.

5.2 Methods

5.2.1 Overview

Two different but related experiments were conducted, one in a Magnetic Resonance Imaging (MRI) scanner and the other in the laboratory. The experiment conducted in the MRI scanner focused on measuring the arterial blood flow measurement with the application of various loads, in addition to providing cross sectional anatomical data which was used in measuring soft tissue thickness. The perfusion experiment performed in the laboratory aimed at determining the superficial skin perfusion changes due to various loads at two different skin temperatures.

5.2.2 PC-MRI Experiment

(i) Arterial and venous blood flow measurement

This study employed the principle of Phase-Contrast Magnetic Resonance Imaging (PC-MRI) to measure blood flow in the artery of the forearm. PC-MRI involves separating signals produced by flowing materials from signals produced by static material in the body, to quantify velocity of blood flow in vessels. This method has been studied and validated by other researchers (Elkins and Alley, 2007; Meyer et al., 1993; Radda et al., 1981).

The study included fifteen male participants, ranging in age from 18 to 44 (Ave. 26.3, SD 7.8) years. All participants voluntarily signed a consent form to participate in the IRB approved research (IRB# 10-1304).

Each participant was positioned prone inside the MRI scanner bed. A smaller MRI coil was placed inside the scanner, and the subject's right forearm was slid into this coil. The purpose of the MRI coil was to improve image resolution. A blood pressure cuff (Dura-cuf REF 2779 by Johnson & Johnson, New Brunswick, NJ) was folded and placed between the arm and the coil. When inflated, the cuff applied a normal load on top of the forearm. To produce shear loads, a weight of 20 N was suspended to one end of a rope, the other end of which was connected to a one-inch webbing wrapped around the wrist securely. The friction between the webbing and skin applied a uniform shear load to the skin. The load application at the end of the rope was made possible using a non-conducting, non-metallic, non-magnetic pulley-weight system, suitable for the MRI setting.

The experiment involved three loading conditions — baseline, normal load, and combined (normal plus shear) load. No loads were applied on the forearm during the baseline condition; however PC-MRI blood flow data were collected. To apply a normal load, the pressure cuff was inflated to 20 mm Hg, and once stable, PC-MRI data were collected and then the cuff was deflated. To apply combined normal and shear loads, the cuff was inflated to 20 mm Hg and a shear load was applied using the pulley-weight system. Blood flow data were recorded. The load magnitudes were selected based on preliminary research and previous studies (Bush and Hubbard, 2007; Manorama et al., 2010).

The order of the conditions was such that the first condition was always the baseline, whereas the other two conditions were alternated across participants. A resting time of five minutes was allowed between the second and the third conditions, during which no loads were applied. After the three conditions were completed, a time-of-flight (TOF) scan which yielded detailed anatomical images was conducted with no load on the forearm. The outputs of the TOF scans were used to measure soft tissue thickness. Finally, the contact area of the pressure cuff on the forearm was determined using a dyeing procedure in which the participants placed their forearm in a replica of the MRI coil while a dyed pressure cuff was inflated to 20 mm Hg. This left an inked marking on the skin, identifying the contact area. This value was used to calculate normal force applied on the forearm in Newtons.

From the PC-MRI data, vessel area segmentation and velocity measurements were made for the anterior interosseous artery (AIOA) using the software Winvessel (Meyer et al., 1993). The blood flow rates were calculated from the velocities and cross-sectional areas for all three loading conditions.

(ii) Soft tissue thickness measurement

The TOF scans from the PC-MRI study were analyzed to obtain the soft tissue thicknesses. The TOF cross-sectional slice pertaining to the midpoint of the scanned area of each subject's forearm was used to obtain the soft tissue thickness data. Using digital image measurement tools (Adobe Systems Inc., San Jose, CA, USA), four sets of data were collected from each participant (Figure 5-1): 1) forearm cross sectional height at mid-plane (MH), 2) forearm cross sectional width at mid-plane (MW), 3) soft tissue thickness from AIOA to the lower surface of forearm in the direction of force application (STT_Y), and 4) soft tissue thickness from AIOA to ulnar side of forearm perpendicular to the direction of force application (STT_X). Specifically, these measurements represented the thickness of the soft tissue (i.e. muscle, skin, and fat) in the horizontal and vertical axes in the MRI slice, and also the horizontal and vertical distances of the AIOA from the outer boundary of the forearm. The distances were measured relative to the AIOA since the focus of the study was to relate soft tissue thickness to arterial blood flow.

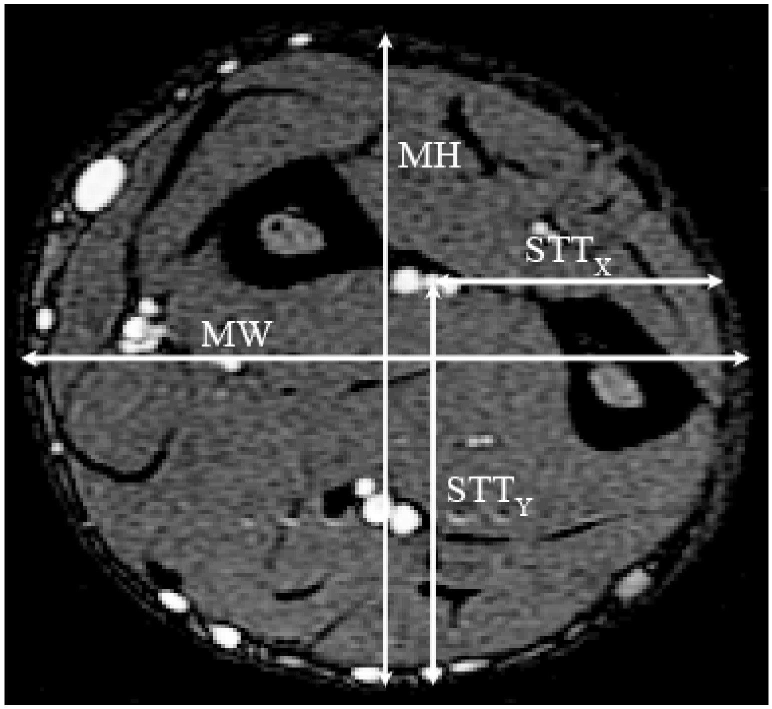

Figure 5-1: A MRI cross sectional slice showing the soft tissue thickness (corresponding to skin, muscle, and fat tissue) measurements. In addition to measuring thickness in horizontal and vertical axes, the distances from ends of the forearm to AIOA were measured.

5.2.3 Skin perfusion measurement

The goal of this experiment was to determine the effects that local skin temperature changes had on skin perfusion at various loads. Two skin temperatures, 44 °C and 37 °C, were tested on seven of the fifteen participants from the PC-MRI experiment who were able to return to the laboratory.

The experimental setup and protocol were designed to imitate the PC-MRI experiment, with a few minor differences. First, the testing was conducted on a padded medical treatment table in the lab, instead of inside a MRI scanner. Secondly, a Laser Doppler Perfusion Monitoring (LDPM) system measured the changes in skin perfusion with different loads, as opposed to monitoring deep vessel flow. The probe used for this study was a non-invasive thermostatic laser doppler probe (Number 457 Probe, Perimed Instruments, Stockholm, Sweden) with a diameter of 10 mm, and was applied to the skin with a medical adhesive. For this kind of probe, the measuring depth has been reported to be between 0.5 and 1 mm (Humeau et al., 2007).

After having the participant lie prone on a padded treatment table and positioning the right forearm inside a replica of the MRI coil, the same setup that was used in the PC-MRI experiments was used to apply normal and shear loads (Figure 5-2). The laser doppler probe was placed on the forearm at the midpoint of the length of the coil, and measurements of probe location were taken. The coil was attached to a multi-axis load cell which measured the forces in three directions. Once the experimental setup was complete, the temperature at the probe surface was set to 44 °C.

The test protocol consisted of three conditions— baseline, normal load, and combined loads. The loads were applied in an identical manner to the PC-MRI experiment. The perfusion data were continuously recorded using LDPM for the entire one minute of each condition. Like the PC-MRI experiment, the order of the second and third conditions was alternated across participants and tests were separated by a resting time of five minutes. The blood perfusion values were averaged over the minute for each condition and were compared across the loading conditions.

The same seven participants returned to the lab for a third set of tests. In this final testing, the probe was heated to a temperature of 37 °C while all other parameters remained the same.

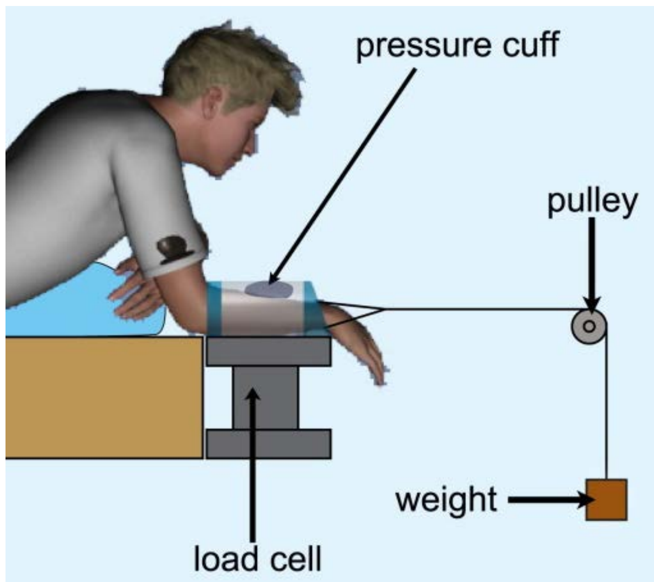

Figure 5-2: Load application in perfusion experiment. Normal loads were applied using the pressure cuff; shear loads were applied using the pulley-weight system. The laser doppler probe (not seen in figure) was placed between the pressure cuff and forearm.

5.3 Results

5.3.1 Relating deep vessel blood flow to soft tissue thickness

Results of the PC-MRI experiment showed an overall trend of decreasing blood flow from baseline to normal load condition, and a further decrease in the condition of combined loading. However, even though the sample as a whole demonstrated this trend, some participants did not exhibit this trend.

The subjects were grouped into two categories— those who did not show a decrease in arterial blood flow from normal to combined load application in the PC-MRI experiment, and those who did. The four measurements of forearm soft tissue thickness in our study, namely MH, MW, STT_Y, and STT_X were statistically compared between subjects. The results showed that the magnitude of average values for all four soft tissue thickness measurements were smaller in individuals who showed a blood flow decrease with application of shear force, than in those who did not show a decrease (Table 5-1)(Figure 5-3).

When statistically compared using a t-test, significance ($p=0.06$ at 90% CI) was obtained for the comparison involving STT_Y. Although statistical significance was not obtained for the other comparisons, medium to high effect sizes ranging from 0.3 to 0.7 were obtained from all comparisons. These results indicated that subjects who showed decreasing blood flow trends with the application of combined loads had lower soft tissue thicknesses.

In order to eliminate the possibility that the decrease in blood flow could have been due to higher magnitudes of shear forces applied and not necessarily due to lower magnitudes of soft tissue thicknesses, the shear forces in the two groups were compared. It was determined that the average shear force applied by participants who showed an arterial blood flow decrease from normal to combined loading condition were, in fact, lower in magnitude (4.4 N) than that of the participants who did not show a decrease (7.0 N). Also, the BMI of participants who showed a decreasing blood flow trend were lower (22.3) than of those who did not show a decreasing blood flow trend (24.0).

Table 5-1: Soft tissue thickness comparison (average and standard deviation) of subjects who showed a blood flow decrease due to shear and those who did not show a decrease.

Soft tissue thickness measurement	Non-decreasing blood flow trend due to shear (n=6)	Decreasing blood flow trend due to shear (n=9)
MH (cm)	7.2 (0.2)	6.9 (0.7)
MW (cm)	7.8 (0.6)	7.5 (0.7)
STT_Y (cm)	4.1 (0.3)	3.7 (0.3)
STT_X (cm)	3.2 (0.2)	3.1 (0.4)

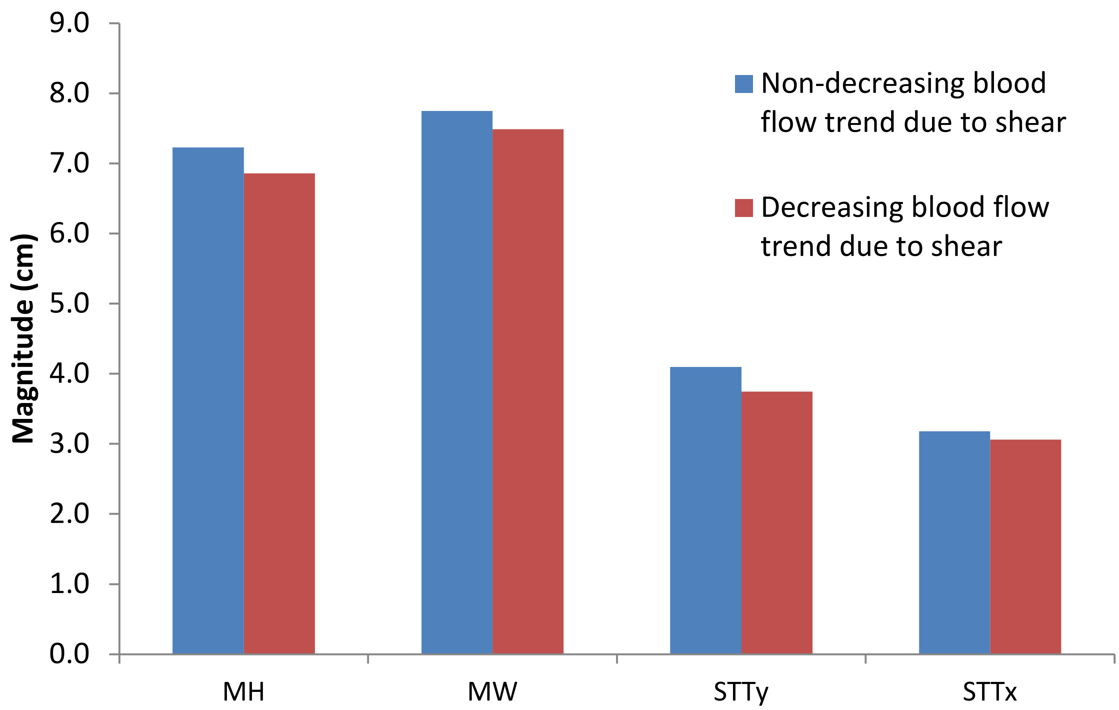

Figure 5-3: Soft tissue thickness comparison of subjects who showed blood flow decrease due to shear and those who did not show a decrease

5.3.2 Evaluation of skin temperature effects on perfusion

The applied normal force during the perfusion experiment was determined as the product of the applied pressure and the contact area, and was calculated as 18 N on an average among all subjects. The shear force was obtained from load cell measurements and on an average was measured to be 8.7 N.

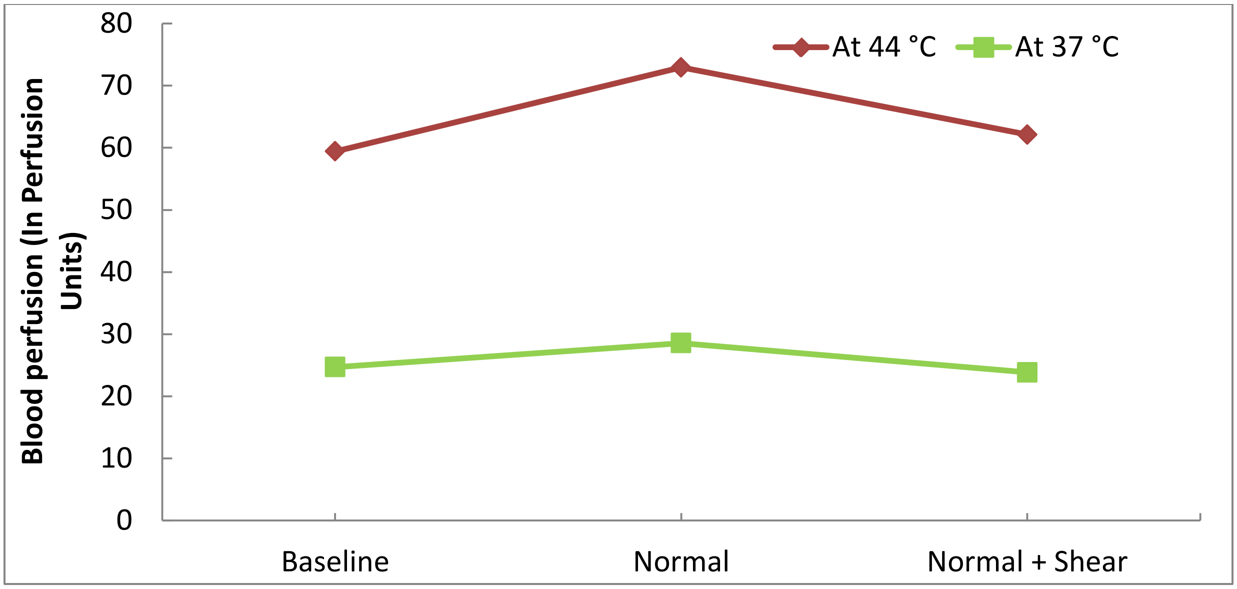

Figure 5-4: Effects of skin temperature on blood perfusion under different loads. Blood perfusion decreased from normal to combined loading at both skin temperatures, but the slope of decrease was higher at 44 °C than at 37 °C.

The tests conducted at 44 °C showed a similar trend in perfusion change to those conducted at 37 °C (Figure 5-4). Specifically, the perfusion increased from baseline to normal, and decreased from normal to combined loading condition. A limitation of the LDPM technique is that it does not allow measurements of perfusion in absolute units. Rather, the measurements are made in arbitrary units called perfusion units, which do not have the same baseline during each testing (Leahy et al., 1999). However, it can measure the changes in perfusion. Hence, the slopes of perfusion change from normal to combined load conditions at the two temperatures were calculated. This slope was found to have a value of -10.8 in tests conducted at 44 °C, which was steeper than the corresponding slope of -4.7 at 37 °C. These results signified that the addition of shear load decreased the skin perfusion, and this decrease was more pronounced at 44 °C than it was at 37 °C.

5.4 Discussion and Conclusions

This study focused on analyzing the relationship between soft tissue thickness and arterial blood flow changes with varied loads, in addition to measuring the effects of local skin temperature on perfusion changes with varied loading conditions.

When measurements of soft tissue thicknesses were compared, it was determined that the average soft tissue thickness measurements were lower in participants who showed an arterial blood flow decrease from normal to combined loading condition than those who did not show a decrease.

These data indicated that subjects with a lower soft tissue thickness showed a greater decrease in blood flow when shear forces were added to normal forces, and thus might be at a greater risk for tissue damage and pressure ulcers. This finding is supportive of a previous study (Clark et al., 1989), which studied the soft tissue thickness of the ischial tuberosity and suggested soft tissue thickness could be a predictor for risk of developing pressure ulcers. However, the results of our study went one step further and explored the relation between soft tissue thickness and blood flow under normal and shear forces, and concluded that shear force caused greater decrease in blood flow in subjects with lower soft tissue thickness.

The perfusion experiment was conducted in a replication of the PC-MRI experimental setup, and measured blood perfusion at two different probe temperatures (44 °C and 37 °C). The results of the tests, at both temperatures, showed an increasing trend from baseline to normal loading and a decreasing trend from normal to combined loading condition. One of our previous studies focused on effects of shear loads on superficial skin perfusion in the seated position, and found a decrease in perfusion from baseline to normal, and a further decrease from normal to shear loading conditions (Manorama et al., 2010). Thus, the results of the comparisons between normal and combined loading conditions from the current study were in accordance to our previous perfusion study. However, the perfusion trend from baseline to normal loading condition was not similar, as there was a decreasing trend in our previous study. This may be due to the fact that in the previous study the loads were subject-specific, whereas in this study the loads were fixed for all subjects, and different subjects respond differently to a specific load.

When perfusion values from normal to combined loading conditions were compared via slope changes at the two temperatures, it was found that the decrease was more at 44 °C than at 37 °C. Thus, shear force, in addition to an elevated temperature is more detrimental than just an elevated temperature to blood flow. This may be due to the fact that an increase in temperature raises the metabolic activity of the tissues. This could lead to the perfusion needs of the tissue not being met, and thus to ischemia and tissue necrosis (Clark et al., 2010; Fisher et al., 1978). When shear force is applied in addition to normal force, the perfusion decreases even further, thus putting the individual at a greater risk for tissue necrosis and PU development.

It should be noted that in the temperature study, only the skin surface below the probe was heated to the specific temperature, and not the entire body segment. The blood perfusion values were also monitored at the same region. The results showed a relationship between local skin temperature and blood perfusion which could be linked to tissue damage. A previous study also found relationships between external pressure and tissue damage at various localized temperature changes, but did not include the effect of shear forces (Kokate et al., 1995). However, a possible limitation of both these studies is that the findings are particular to the local region, and cannot be extended to the entire body segment.

This study is the first to analyze the combined effects of shear forces with other factors related to PU development. Specifically, the relationships of soft tissue thickness and skin temperature with blood flow changes were evaluated at normal and combined loads. The findings of this study are a valuable addition to the knowledge related to pressure ulcer development, since they indicate that a person's susceptibility to develop a PU would increase when experiencing shear loads in addition to having a lower soft tissue thickness, or when exposed to shear loads at warmer temperatures. In conclusion, this study emphasizes the importance of considering the combining effects of factors while designing ulcer prevention measures.

6. CONCLUSIONS

This research aimed at gaining a better overall understanding of the effects of shear force on arterial and venous blood flow and skin perfusion, as well as deformation and internal stresses in the tissues, through a combination of experimental and modeling approaches. It also explored the relationships of soft tissue thickness and skin temperature with blood flow changes at various loads. In addition, it provided a novel approach to model arterial to venous blood flow using porous media.

The results of the PC-MRI experiments showed that shear force was more detrimental to arterial and venous blood flow, than normal force alone. Prior research showed that shear forces applied to the skin caused a decrease in superficial skin perfusion, more so than increasing the normal forces alone. However, it was not clear until now if these superficially applied loads affected only the perfusion at the skin or if they also affected deep vessel blood flow. Thus, the results of the PC-MRI experiments made it clear that combined forces of normal and shear affected not only the superficial skin perfusion, but also the blood flow at the deeper arterial and venous levels. This is an important finding because decreased blood flow to a region can lead to tissue necrosis and a pressure ulcer. Therefore, shear forces applied at the skin level are an important factor to consider when studying blood flow changes in relation to pressure ulcers. Also, the results showing that external forces decreased the deeper vessel blood flow and also the superficial skin perfusion support both theories of tissue damage initiation— pressure ulcers could initiate superficially, and also at a deeper level as a result of reduced blood flow.

The structural deformation analysis conducted with the FE model showed that the externally applied shear affected the internal stresses and deformation in the skin and muscle tissues by creating higher stresses than those due to normal forces alone. The results provided insight into the mode of pressure ulcer formation by suggesting that tissue necrosis, and thus pressure ulcers could initiate due to deformation of the tissues, and not just due to a decrease in blood flow. In addition, the results suggested that tissue necrosis was likely to occur at the bone-muscle interface and also at the skin level since both regions showed higher stress levels, particularly with the addition of shear forces. Thus, tissue damage initiation could start at the deeper level and proceed outwards, and also start at the skin level and proceed inwards.

The new approach developed and demonstrated to simulate vascular flow in the forearm as a system modeled the arterial to venous blood flow by assuming muscle tissue to be permeable to blood flow. With this approach, the complexities of modeling the entire vascular network were removed, and replaced with a permeable media material. The results of this approach and application showed that when muscle was assumed to be permeable to blood flow, the permeability decreased with the application of normal load, and decreased further when shear forces were added. This approach of modeling will provide useful information in pressure ulcer research, which cannot be achieved with experimental testing. For instance, the PC-MRI experiments quantified the effects of external forces on blood flow only at the arteries and veins. However, by modeling all arteries and veins and simulating the blood flow using this approach, the effective blood flow change at any region of the cross section can be determined as a function of loading. This knowledge will be useful in furthering our understandings with regard to tissue regions that are at higher risk for tissue necrosis. This information is a necessity for progress towards improving measures of ulcer prevention.

The blood flow data from PC-MRI experiments when related with the corresponding soft tissue thickness of participants indicated that those who showed a decrease in blood flow when shear loads were applied had smaller magnitudes of soft tissue thicknesses. Another set of experiments studying the effects of normal and combined loads on skin perfusion at two different local skin temperatures indicated that a larger decrease in perfusion occurred at an elevated temperature. Soft tissue thickness and local skin temperature are factors associated with the development of pressure ulcers. The results of this study suggested that an individual would be more susceptible to developing an ulcer when experiencing shear loads in addition to having a lower soft tissue thickness, or when exposed to shear loads at a warmer temperature. For example, slender people with low BMI are believed to be at a higher risk of pressure ulcers. But when a slender person experiences shear forces while seated, the risk for developing pressure ulcers could be even higher. Similarly, increased skin temperature is a recognized factor leading to pressure ulcers. But this research indicates that increased skin temperature in addition to experiencing shear loads increases the risk further. Thus, these results were important in that they explored the combination of factors related to blood flow which is directly linked to tissue necrosis.

Future work will focus on parallel experimental and modeling work for other ulcer-prone regions such as the ischial or the sacral region using PC-MRI and LDPM. Further development of the permeability model is also necessary. Model additions will include all measureable vessels of the body segment, in comparison to the single artery and vein modeled currently. The addition of these vessels will also allow for the evaluation of sub- regions in the cross-sectional slice.

In conclusion, this research is a foundation for future research related to evaluation of blood flow, skin perfusion, internal stresses and deformation due to applied external loads, helping us identify criteria related to pressure ulcer susceptibility. The knowledge gained from this research will be instrumental in achieving the ultimate goal of reducing the prevalence rates of pressure ulcers.

BIBLIOGRAPHY

BIBLIOGRAPHY

Agache, P.G., Monneur, C., Leveque, J.L., De Rigal, J., 1980. Mechanical properties and Young's modulus of human skin in vivo. Arch. Dermatol. Res. 269, 221–232.

Agam, L., Gefen, A., 2007. Pressure ulcers and deep tissue injury: a bioengineering perspective. J. Wound Care 16, 336–342.

Alam, K., Anghelescu, M.S., Bradu, A., 2011. Computational model of porous media using true 3-D images, in: Heat Transfer in Multi-Phase Materials. Springer, pp. 347–377.

Autodesk, 2013. Autodesk Simulation CFD.

Back, L.H., Radbill, J.R., Crawford, D.W., 1977. Analysis of oxygen transport from pulsatile, viscous blood flow to diseased coronary arteries of man. J. Biomech. 10, 763–774.

Baharestani, M.M., Black, J.M., Carville, K., Clark, M., Cuddigan, J.E., Dealey, C., Defloor, T., Harding, K.G., Lahmann, N.A., Lubbers, M.J., Lyder, C.H., Ohura, T., Orsted, H.L., Reger, S.I., Romanelli, M., Sanada, H., 2009. Dilemmas in measuring and using pressure ulcer prevalence and incidence: An international consensus. Int. Wound J. 6, 97–104.

Baharestani, M.M., Ratliff, C.R., 2007. Pressure Ulcers in Neonates and Children: An NPUAP White Paper. Adv. Ski. Wound Care 20, 208–220.

Baish, J.W., Netti, P.A., Jain, R.K., 1997. Transmural coupling of fluid flow in microcirculatory network and interstitium in tumors. Microvasc. Res. 53, 128–141.

Balar, S.D., Rogge, T.R., Young, D.F., 1989. Computer simulation of blood flow in the human arm. J. Biomech. 22, 691–7.

Bansal, C., Scott, R., Stewart, D., Cockerell, C.J., 2005. Decubitus ulcers: A review of the literature. Int. J. Dermatol. 44, 805–810.

Bear, J., 2013. Dynamics of fluids in porous media. DoverPublications. com.

Bennett, G., Dealey, C., Posnett, J., 2004. The cost of pressure ulcers in the UK. Age Ageing 33, 230–235.

Bennett, L., Kavner, D., Lee, B.K., Trainor, F.A., 1979. Shear vs pressure as causative factors in skin blood flow occlusion. Arch. Phys. Med. Rehabil. 60, 309–314.

Bergstrom, N., Allman, R., Carlson, C., 1992. Clinical Practice Guideline Number 3: Pressure Ulcers in Adults: Prediction and Prevention. Public Health Service, US Dept of Health and Human Services, Rockville, MD.

Bergstrom, N., Braden, B., 1992. A prospective study of pressure sore risk among institutionalized elderly. J. Am. Geriatr. Soc. 40, 747–758.

Bouten, C. V, Oomens, C.W., Baaijens, F.P., Bader, D.L., 2003. The etiology of pressure ulcers: skin deep or muscle bound? Arch. Phys. Med. Rehabil. 84, 616–619.

Brem, H., Lyder, C., 2004. Protocol for the successful treatment of pressure ulcers. Am. J. Surg. 188, 9–17.

Breuls, R.G.M., Bouten, C.V.C., Oomens, C.W.J., Bader, D.L., Baaijens, F.P.T., 2003. Compression Induced Cell Damage in Engineered Muscle Tissue: An In Vitro Model to Study Pressure Ulcer Aetiology. Ann. Biomed. Eng. 31, 1357–1364.

Brienza, D.M., Geyer, M.J., 2005. Using Support Surfaces to Manage Tissue Integrity. Adv. Skin Wound Care 18, 151–157.

Brillhart, B., 2005. Pressure sore and skin tear prevention and treatment during a 10-month program. Rehabil. Nurs. 30, 85–91.

Brooks, B., 1922. Pathologic changes in muscle as a result of disturbances of circulation: An experimental study of volkmann's ischemic paralysis. Arch. Surg. 5, 188–216.

Bush, T.R., Hubbard, R., 2007. Support force measures of midsized men in seated positions. J. Biomech. Eng. 129, 58–65.

Butler, S.L., Kohles, S.S., Thielke, R.J., Chen, C., Vanderby Jr, R., 1997. Interstitial fluid flow in tendons or ligaments: a porous medium finite element simulation. Med. Biol. Eng. Comput. 35, 742–746.

Carr, M.E., Shen, L.L., Hermans, J., 1977. Mass–length ratio of fibrin fibers from gel permeation and light scattering. Biopolymers 16, 1–15.

Cebral, J.R., Yim, P.J., Löhner, R., Soto, O., Choyke, P.L., 2002. Blood flow modeling in carotid arteries with computational fluid dynamics and MR imaging. Acad. Radiol. 9, 1286–1299.

Chabanas, M., Payan, Y., 2000. A 3D Finite Element Model of the Face for Simulation in Plastic and Maxillo-Facial Surgery, in: Medical Image Computing and Computer-Assisted Intervention–MICCAI 2000. pp. 1068–1075.

Chow, W., Odell, E., 1978. Deformation and stresses in soft body tissues of a sitting person. J. Biomech. Eng. 100, 79–87.

Clark, M., Bours, G., Defloor, T., 2004. Pressure Ulcers: Recent Advances in Tissue Viability. Quay Books, Salisbury.

Clark, M., Romanelli, M., Reger, S., Ranganathan, V., Black, J., Dealey, C., 2010. Microclimate in context. International guidelines. Pressure ulcer prevention: pressure, shear, friction and microclimate in context. A consensus document. London Wounds Int. 19–25.

Clark, M., Rowland, L.B., Wood, H. a, Crow, R. a, 1989. Measurement of soft tissue thickness over the sacrum of elderly hospital patients using B-mode ultrasound. J. Biomed. Eng. 11, 200–202.

Coccagna, G., Mantovani, M., Brignani, F., Manzini, A., Lugaresi, E., 1971. Arterial pressure changes during spontaneous sleep in man. Electroencephalogr. Clin. Neurophysiol. 31, 277–281.

Cohen, J., 1988. Statistical Power Analysis for the Behavioral Sciences, 2nd ed. Routledge.

Cuddigan, J., Berlowitz, D.R., Ayello, E.A., Elizabeth, A., 2001. Pressure ulcers in America: Prevalence, Incidence, and Implications for the Future: An Executive Summary of the National Pressure Ulcer Advisory Panel Monograph. Adv. Skin Wound Care 14, 4.

Curley, M.A.Q., Razmus, I.S., Roberts, K.E., Wypij, D., 2003. Predicting Pressure Ulcer Risk in Pediatric Patients: The Braden Q Scale. Nurs. Res. 52, 22–33.

Darcy, H., 1856. Les fontaines publiques de la ville de Dijon. Victor Dalmont.

Ehrlich, L.W., Friedman, M.H., 1977. Steady convective diffusion in a bifurcation. Biomed. Eng. IEEE Trans. 12–18.

Elango, L., Sivakumar, C., 2005. Numerical Simulation of Groundwater Flow and Solute Transport, Numerical Simulation of Groundwater Flow and Solute Transport. Allied Publishers, Chennai.

Elkins, C.J., Alley, M.T., 2007. Magnetic resonance velocimetry: applications of magnetic resonance imaging in the measurement of fluid motion. Exp. Fluids 43, 823–858.

El-Shahed, M., 2003. Pulsatile flow of blood through a stenosed porous medium under periodic body acceleration. Appl. Math. Comput. 138, 479–488.

EPUAP, 2009. Prevention and treatment of pressure ulcers: quick reference guide. Washingt. DC, USA Natl. Press. Ulcer Advis. Panel.

Fisher, S. V, Szymke, T.E., Apte, S.Y., Kosiak, M., 1978. Wheelchair cushion effect on skin temperature. Arch. Phys. Med. Rehabil. 59, 68.

Fournier, R., 2011. Basic Transport phenomena in Biomedical Engineering, 3rd ed. CRC press.

Fujioka, M., Yakabe, A., Masuda, K., Imamura, Y., 2010. Unusual cheek and upper extremity pressure ulcers resulting from head-on hand and arm napping. Wounds. 22, 127–131.

Fung, Y.C., 1993. Biomechanics : mechanical properties of living tissues, 2nd ed. Springer-Verlag, New York.

Gawlitta, D., Li, W., Oomens, C.W., Baaijens, F.P., Bader, D.L., Bouten, C. V, 2007a. The relative contributions of compression and hypoxia to development of muscle tissue damage: an in vitro study. Ann. Biomed. Eng. 35, 273–284.

Gawlitta, D., Oomens, C.W., Bader, D.L., Baaijens, F.P., Bouten, C. V, 2007b. Temporal differences in the influence of ischemic factors and deformation on the metabolism of engineered skeletal muscle. J. Appl. Physiol. 103, 464–473.

Gefen, A., 2007. Risk factors for a pressure-related deep tissue injury: a theoretical model. Med. Biol. Eng. Comput. 45, 563–573.

Gefen, A., van Nierop, B., Bader, D.L., Oomens, C.W., 2008. Strain-time cell-death threshold for skeletal muscle in a tissue-engineered model system for deep tissue injury. J. Biomech. 41, 2003–2012.

Gilsdorf, P., Patterson, R., Fisher, S., Appel, N., 1990. Sitting forces and wheelchair mechanics. J. Rehabil. Res. Dev. 27, 239–246.

Goldstein, B., Sanders, J., 1998. Skin response to repetitive mechanical stress: a new experimental model in pig. Arch. Phys. Med. Rehabil. 79, 265–272.

Goossens, R.H., Snijders, C.J., Holscher, T.G., Heerens, W.C., Holman, A.E., 1997. Shear stress measured on beds and wheelchairs. Scand. J. Rehabil. Med. 29, 131–136.

Goossens, R.H., Zegers, R., Hoek van Dijke, G.A., Snijders, C.J., 1994. Influence of shear on skin oxygen tension. Clin. Physiol. 14, 111–118.

Grobelnik, B., Vidmar, J., Tratar, G., Blinc, A., Sersa, I., 2008. Flow-induced permeation of non-occlusive blood clots: an MRI study and modelling. Eur. Biophys. J. 37, 1229–1233.

Hall, C., Hoff, W.D., 2009. Water transport in brick, stone and concrete. CRC Press.

Hobson, D.A., 1992. Comparative effects of posture on pressure and shear at the body-seat interface. J. Rehabil. Res. Dev. 29, 21–31.

Huberty, C.J., 1987. On Statistical testing. Educ. Res. 16, 4–9.

Humeau, A., Steenbergen, W., Nilsson, H., Strömberg, T., 2007. Laser Doppler perfusion monitoring and imaging: novel approaches. Med. Biol. Eng. Comput. 45, 421–35.

Hunt, M.L., Tien, C.L., 1988. Effects of thermal dispersion on forced convection in fibrous media. Int. J. Heat Mass Transf. 31, 301–309.

Huyghe, J.M., Arts, T., van Campen, D.H., Reneman, R.S., 1992. Porous medium finite element model of the beating left ventricle. Am. J. Physiol. 262, H1256–H1267.

Kaltenthaler, E., Withfield, M., Walters, S., Akehurst, R., Paisley, S., 2001. UK, USA and Canada: how do their pressure ulcer prevalence and incidence data compare? J. Wound Care. 10, 530–535.

Karner, G., Perktold, K., Zehentner, H.P., Prosi, M., 2000. Mass transport in large arteries and through the artery wall. Adv. Fluid Mech. 23, 209–248.

Kenner, T., 1989. The measurement of blood density and its meaning. Basic Res. Cardiol. 84, 111–124.

Keys, K.A., Daniali, L.N., Warner, K.J., Mathes, D.W., 2010. Multivariate Predictors of Failure after Flap Coverage of Pressure Ulcers. Plast. Reconstr. Surg. 125, 1725–1734.

Kokate, J., Leland, K., Held, A., 1995. Temperature-modulated pressure ulcers: a porcine model. Arch. Phys. Med. Rehabil. 76, 666–673.

Kosiak, M., 1959. Etiology and pathology of ischemic ulcers. Arch. Phys. Med. Rehabil. 40, 62–69.

Kosiak, M., 1961. Etiology of decubitus ulcers. Arch. Phys. Med. Rehabil. 42, 19–29.

Kosiak, M., Kubicek, W.G., Olson, M., Danz, J.N., Kottke, F.J., 1958. Evaluation of pressure as a factor in the production of ischial ulcers. Arch. Phys. Med. Rehabil. 39, 623–629.

Kottner, J., Gefen, A., Lahmann, N., 2011. Weight and pressure ulcer occurrence: A secondary data analysis. Int. J. Nurs. Stud. 48, 1339–1348.

Ku, D.N., 1997. Blood flow in arteries 399–434.

Labovitz, S., 1968. Criteria for Selecting a Significance Level : A Note on the Sacredness of . 05. Am. Sociol. 3, 220–222.

Lachenbruch, C., 2005. Skin cooling surfaces: Estimating the importance of limiting skin temperature. Ostomy wound Manag. 51, 70–79.

Lahmann, N.A., Halfens, R.J.G., Dassen, T., 2005. Prevalence of pressure ulcers in Germany. J. Clin. Nurs. 14, 165–172.

Lazarus, G.S., Diane, M., Knighton, D.R., David, J., Rodeheaver, G., Robson, M.C., 1994. Defintions and Guidelines for Assessment of Wounds and Evaluation of Healing. Arch. Dermatol. 130, 489–493.

Leahy, M.J., De Mul, F.F., Nilsson, G.E., Maniewski, R., 1999. Principles and practice of the laser-Doppler perfusion technique. Technol. Heal. care 7, 143–62.

Linder-Ganz, E., Engelberg, S., Scheinowitz, M., Gefen, A., 2006. Pressure-time cell death threshold for albino rat skeletal muscles as related to pressure sore biomechanics. J. Biomech. 39, 2725–2732.

Linder-Ganz, E., Gefen, A., 2004. Mechanical compression-induced pressure sores in rat hindlimb: muscle stiffness, histology, and computational models. J. Appl. Physiol. 96, 2034–2049.

Linder-Ganz, E., Gefen, A., 2007a. The effects of pressure and shear on capillary closure in the microstructure of skeletal muscles. Ann. Biomed. Eng. 35, 2095–2107.

Linder-Ganz, E., Gefen, A., 2007b. The effects of pressure and shear on capillary closure in the microstructure of skeletal muscles. Ann. Biomed. Eng. 35, 2095–107.

Linder-Ganz, E., Shabshin, N., Itzchak, Y., Gefen, A., 2007. Assessment of mechanical conditions in sub-dermal tissues during sitting: a combined experimental-MRI and finite element approach. J. Biomech. 40, 1443–1454.

Lyder, C.H., 2003. Pressure ulcer prevention and management. JAMA J. Am. Med. Assoc. 289, 223–226.

Makhsous, M., Lim, D., Hendrix, R., Bankard, J., Rymer, W.Z., Lin, F., 2007. Finite element analysis for evaluation of pressure ulcer on the buttock: development and validation. Neural Syst. Rehabil. Eng. IEEE Trans. on, 15, 517–525.

Manorama, A., Meyer, R., Wiseman, R., Bush, T.R., 2013. Quantifying the effects of external shear loads on arterial and venous blood flow: Implications for pressure ulcer development. Clin. Biomech. 28, 574–578.

Manorama, A.A., Baek, S., Vorro, J., Sikorskii, A., Bush, T.R., 2010. Blood perfusion and transcutaneous oxygen level characterizations in human skin with changes in normal and shear loads — Implications for pressure ulcer formation. Clin. Biomech. 25, 823–828.

McLane, K.M., Bookout, K., McCord, S., McCain, J., Jefferson, L.S., 2004. The 2003 National Pediatric Pressure Ulcer and Skin Breakdown Prevalence Survey: A Multisite Study. J. Wound Ostomy Cont. Nurs. 31, 168–178.

Meyer, R.A., Foley, J.M., Harkema, S.J., Sierra, A., Potchen, E.J., 1993. Magnetic resonance measurement of blood flow in peripheral vessels after acute exercise. Magn. Reson. Imaging 11, 1085–1092.

Mimura, M., Ohura, T., Takahashi, M., Kajiwara, R., Ohura, N., 2009. Mechanism leading to the development of pressure ulcers based on shear force and pressures during a bed operation: influence of body types, body positions, and knee positions. Wound Repair Regen. 17, 789–796.

Nakayama, a., Kuwahara, F., 2008. A general bioheat transfer model based on the theory of porous media. Int. J. Heat Mass Transf. 51, 3190–3199.

Nhs.uk, 2009. NHS Institute for Innovation and Improvement [WWW Document]. URL http://www.institute.nhs.uk

Nixon, J., Brown, J., McElvenny, D., 2000. Prognostic factors associated with pressure sore development in the immediate post-operative period. Int. J. Nurs. Stud. 37, 279–284.

Nola, G.T., Vistnes, L.M., 1980. Differential response of skin and muscle in the experimental production of pressure sores. Plast. Reconstr. Surg. 66, 728–733.

Nordez, A., Hug, F., 2010. Muscle shear elastic modulus measured using supersonic shear imaging is highly related to muscle activity level. J. Appl. Physiol. 108, 1389–1394.

NPUAP, 2009. Prevention and treatment of pressure ulcers: Clinical practice guideline. Washingt. DC Natl. Press. Ulcer Advis. Panel.

Ochsner, A., Colp, R., Burch, G.E., 1951. Normal Blood Pressure in the Superficial Venous System of Man at Rest in the Supine Position. Circulation 3, 674–680.

Olesen, C.G., de Zee, M., Rasmussen, J., 2010. Missing links in pressure ulcer research: An interdisciplinary overview. J. Appl. Physiol. 108, 1458–1464.

Oomens, C.W.J., Bressers, O.F.J.T., Bosboom, E.M.H., Bouten, C.V.C., Bader, D.L., 2003. Can Loaded Interface Characteristics Influence Strain Distributions in Muscle Adjacent to Bony Prominences? Comput. Methods Biomech. Biomed. Engin. 6, 171–180.

Pailler-Mattei, C., Bec, S., Zahouani, H., 2008. In vivo measurements of the elastic mechanical properties of human skin by indentation tests. Med. Eng. Phys. 30, 599–606.

Parish, L.C., Witkowski, J.A., 2004. Controversies about the decubitus ulcer. Dermatol Clin 22, 87–91.

Peeters, E.A., Bouten, C. V, Oomens, C.W., Baaijens, F.P., 2003. Monitoring the biomechanical response of individual cells under compression: a new compression device. Med. Biol. Eng. Comput. 41, 498–503.

Pollack, A.A., Wood, E.H., 1949. Venous pressure in the saphenous vein at the ankle in man during exercise and changes in posture. J. Appl. Physiol. 1, 649–662.

Portnoy, S., Siev-Ner, I., Shabshin, N., Kristal, A., Yizhar, Z., Gefen, A., 2009. Patient-specific analyses of deep tissue loads post transtibial amputation in residual limbs of multiple prosthetic users. J. Biomech. 42, 2686–2693.

Prosi, M., Zunino, P., Perktold, K., Quarteroni, A., 2005. Mathematical and numerical models for transfer of low-density lipoproteins through the arterial walls: A new methodology for the model set up with applications to the study of disturbed lumenal flow. J. Biomech. 38, 903–917.

Radda, G.K., Styles, P., Thulborn, K.R., Waterton, J.C., 1981. A simple method of flow measurement by pulsed NMR. J. Magn. Reson. 42, 488–490.

Rappitsch, G., Perktold, K., Pernkopf, E., 1997. Numerical modelling of shear-dependent mass transfer in large arteries. Int. J. Numer. methods fluids 25, 847–857.

Reddy, N., Brunski, J., Patel, H., Cochran, G., 1980. Stress distributions in a loaded buttock with various seat cushions. Adv. Bioeng. 97–100.

Reuler, J.B., Cooney, T.G., 1981. The pressure sore: pathophysiology and principles of management. Ann. Intern. Med. 94, 661–666.

Russo, C., Steiner, C., Spector, W., 2008. Hospitalizations related to pressure ulcers among adults 18 years and older, 2006. HCUP Statistical Brief# 64, Agency for Healthcare Research and Quality, Rockville, MD.

Shea, J.D., 1975. Pressure Sores Classification and Management. Clin. Orthop. Relat. Res. 112, 89–100.

Stangeby, D.K., Ethier, C.R., 2002. Computational analysis of coupled blood-wall arterial LDL transport. J. Biomech. Eng. 124, 1–8.

Stekelenburg, A., Gawlitta, D., Bader, D.L., Oomens, C.W., 2008. Deep tissue injury: how deep is our understanding? Arch. Phys. Med. Rehabil. 89, 1410–1413.

Sugarman, B., 1985. Infection and pressure sores. Arch. Phys. Med. Rehabil. 66, 177–179.

Sugarman, B., 1987. Pressure sores and underlying bone infection. Arch. Intern. Med. 147, 553–555.

Sun, Q., Lin, F., Al-Saeede, S., Ruberte, L., Nam, E., Hendrix, R., Makhsous, M., 2005. Finite element modeling of human buttock-thigh tissue in a seated posture, in: Summer Bioengineering Conference. Vail, Colorado, pp. 22–26.

Vanderwee, K., Clark, M., Dealey, C., Gunningberg, L., Defloor, T., 2007. Pressure ulcer prevalence in Europe: a pilot study. J. Eval. Clin. Pract. 13, 227–235.

VanGilder, C., Macfarlane, G., Meyer, S., Lachenbruch, C., 2009. Body Mass Index , Weight , and Pressure Ulcer Prevalence: An analysis of the 2006-2007 International Pressure Ulcer Prevalence Surveys. J. Nurs. Care Qual. 24, 127–135.

Vankan, W.J., Huyghe, J.M., Drost, M.R., Janssen, J.D., Huson, A., 1997. A finite element mixture model for hierarchical porous media. Int. J. Numer. Methods Eng. 40, 193–210.

Vankan, W.J., Huyghe, J.M., Janssen, J.D., Huson, A., 1996. A 3-D Finite Element model of blood prefused rat gastrocnemius medialis muscle. Eur. J. Morphol. 34, 19–24.

Verruijt, A., 1970. Theory of groundwater flow 174–182.

Versluysen, M., 1986. How elderly patients with femoral fracture develop pressure sores in hospital. Br. Med. J. (Clin. Res. Ed). 292, 1311.

Whitney, J., Phillips, L., Aslam, R., Barbul, A., Gottrup, F., Gould, L., Robson, M.C., Rodeheaver, G., Thomas, D., Stotts, N., 2006. Guidelines for the treatment of pressure ulcers. Wound Repair Regen. 14, 663–679.

Woodbury, M., Houghton, P., 2004. Prevalence of pressure ulcers in Canadian healthcare settings. Ostomy Wound Manag. 50, 22–44.

Zadpoor, A.A., 2006. Finite element method analysis of human hand arm vibrations. Int. J. Sci. Res. 16, 391–395.

Zhang, M., Roberts, V.C., 1993. The effect of shear forces externally applied to skin surface on underlying tissues. J. Biomed. Eng. 15, 451–456.

Zhang, M., Roberts, V.C., 1994. The reaction of skin and soft tissue to shear forces applied externally to the skin surface. Proc. Inst. Mech. Eng. Part H J. Eng. Med. 208, 217–222.

Zunino, P., 2002. Mathematical and numerical modeling of mass transfer in the vascular system. PhD thesis, Ecole Polytechnique Fédérale de Lausanne.